NASA TM-84290

NASA Technical Memorandum 84290

NASA-TM-84290 19830005122

An Experimental Documentation of a Separated Trailing-Edge Flow at a Transonic Mach Number

P. R. Viswanath and J. L. Brown

November 1982

NASA
National Aeronautics and
Space Administration

NASA Technical Memorandum 84290

An Experimental Documentation of a Separated Trailing-Edge Flow at a Transonic Mach Number

P. R. Viswanath
J. L. Brown, Ames Research Center, Moffett Field, California

National Aeronautics and
Space Administration

Ames Research Center
Moffett Field. California 94035

N83-13393 #

AN EXPERIMENTAL DOCUMENTATION OF A SEPARATED TRAILING-EDGE FLOW AT A TRANSONIC MACH NUMBER

P. R. Viswanath* and J. L. Brown

Ames Research Center

SUMMARY

A detailed experiment on the separated flow field at a sharp trailing edge is described and documented. The separated flow is a result of sustained adverse pressure gradients. The experiment was conducted using an elongated airfoil-like model at a transonic Mach number and at a high Reynolds number of practical interest. Measurements made include surface pressures and detailed mean and turbulence flow quantities in the region just upstream of separation to downstream into the near-wake, following wake closure. The data obtained are presented mostly in tabular form. These data are of sufficient quality and detail to be useful as a test case for evaluating turbulence models and calculation methods.

NOMENCLATURE

c_f	wall skin-friction coefficient, $2\tau_w/\rho_e U_e^2$
H	shape factor, δ^*/Θ
L	model length, see figure 1
M	Mach number
P	static pressure
P_T or PT	total pressure
Re	Reynolds number per meter based on nominal free-stream conditions
T_T	total temperature
U	mean velocity in X-direction
U_o	sonic (reference) velocity
U^+	law-of-the-wall velocity coordinate, $U/(\tau_w/\rho_w)$
V	mean velocity in Y-direction

---

*Research Associate, Joint Institute for Aeronautics and Acoustics, Stanford University, Stanford, California.

$\langle uv \rangle$	mean velocity correlation
$\langle u^2 \rangle$	mean-square-velocity fluctuation in X-direction
$\langle v^2 \rangle$	mean-square-velocity fluctuation in Y-direction
X	streamwise coordinate parallel to model centerline measured from model trailing edge
Y	vertical coordinate normal to model centerline measured from model surface and in the wake from the model trailing edge
Y^+	law-of-the-wall distance coordinate, $Y(\tau_w \rho_w)^{1/2}/\mu_w$
Z	spanwise coordinate parallel to trailing edge of model and measured from trailing edge at tunnel midspan
γ_p	downstream intermittency
δ	boundary-layer thickness
δ^*	displacement thickness
Θ	momentum thickness
μ	molecular viscosity
ρ	density
τ	shear stress
ϕ	stream function

Subscripts:

e	boundary-layer edge conditions
fr	flow reversal
L	based on model length
n	nominal free-stream conditions
w	wall

INTRODUCTION

There is a continuing need for well-documented experiments on complex turbulent flows for evaluating and improving turbulence modeling, as well as for validating computer codes (ref. 1). At Ames Research Center, there is an on-going program to improve turbulence models for a variety of complex flow fields as applied to external aerodynamics. As a part of this program, trailing-edge and near-wake flows relevant to airfoil applications have been studied in some detail in the last few years.

Symmetric and asymmetric attached trailing-edge flows with pressure gradients upstream of the trailing-edge have been studied at subsonic and low transonic Mach numbers. The results of these investigations are reported in references 2 and 3. The present study deals with a small-scale, trailing-edge separated flow resulting from sustained adverse pressure gradients at a transonic Mach number. This problem is of considerable interest in modern transonic airfoil applications.

The model used in the experiments has a relatively simple geometry that is relevant to practical applications. The free-stream conditions were chosen to avoid the shock on the upper surface of the model, thus reducing flow complexity. Laser-Doppler velocimetry was used for flow diagnostics; it enabled measurements throughout the flow field, including the separated region. The experiment was designed along some of the guidelines suggested in the recent Stanford Conference (ref. 1) to be useful as a test case for evaluating turbulence models and prediction methods.

Results from this investigation, along with a description of the separated flow field and data analysis, are reported in reference 4. Here we describe the experiments in detail and present the data mostly in tabular form. Some of the results are also shown graphically to show the nature of the flow field and variation of the flow quantities.

EXPERIMENTS

Test Facility and Test Conditions

The experiments were conducted in the 38.1 by 25.4-cm High Reynolds Number blowdown facility at Ames Research Center [fig. 1(a)]. The tunnel Mach number can be varied in discrete steps by appropriately choosing the choke inserts located downstream of the test section. Finer control of Mach number is achieved with the help of a translating wedge located in the vicinity of the choke insert.

During the initial phase of the experiments, the free-stream Mach number was varied in order to identify a suitable separated flow for detailed measurements. All flow-field measurements were finally carried out at a nominal free-stream Mach number[1] M_n of 0.7 and at a Reynolds number (based on model length) Re_L of 40×10^6. The nominal total temperature T_T and total pressure P_T of the tests were 470°R and 275×10^3 N/m^2, respectively. The total temperature variation about the nominal value was within ±10°R during the different runs and over the test program period. The total pressure was held constant within $\pm 1.7 \times 10^3$ N/m^2 for different tunnel runs.

---

[1] The nominal Mach number quoted refers to the nearly constant downstream tunnel Mach number estimated (for $X > 30$ cm) from the measured tunnel-wall pressures. Free-stream Mach number is not known precisely since the model leading-edge is close to the entrance section [fig. 1(a)], but it is likely to be slightly less than 0.7 in view of the relatively smaller tunnel-wall boundary-layer displacement thickness effects at the entrance section.

Model Configuration

The model configuration, which spans the test section, is made up of two parts: (1) a forebody, which is a flat plate 56.75 cm long and 2.54 cm thick with a 24.51-cm-long tapered forward section having a rounded leading edge [fig. 1(b)]; and (2) an aftbody, sharp trailing-edge flap, which is 14.1 cm long. The cross section of the flap is the upper rear quadrant of an 18%-thick circular-arc airfoil; the arc has a radius of curvature of 40.4 cm and the trailing-edge-included angle of the flap is 20.4°. The design of the flap was guided by our experience from earlier studies (refs. 2, 3), as well as by some of the criteria for turbulent boundary-layer separation suggested in the literature. The flap can be deflected to any angle within ±20° about $Y = 0$ [see fig. 1(b)], to impose different pressure gradients on the boundary layers. However, for this experiment, the flap was not deflected, thus minimizing the overall complexity of the flow. In the undeflected position, the lower surface of the flap is in line with the lower surface of the flat plate, providing a zero-pressure-gradient turbulent boundary-layer flow. The model has these added advantages: (1) it provides a thick and fully developed turbulent boundary layer on the flat plate, which is desirable for modeling studies, and (2) the relatively long length of the model, combined with the stagnation pressure available with the facility, gives high Reynolds numbers, a unique feature of the present experiments.

Surface Measurements

The flat-plate flap model described above has 75 static-pressure orifices (i.d. = 0.075 cm), most of which are located on the centerline of the model on both the upper and lower surfaces. Spanwise static pressure orifices, in the flat-plate and flap region corresponding to specific streamwise stations on the centerline, were also provided to assess spanwise uniformity of surface pressures. Static-pressure orifices were also provided (at intervals of 10 cm) on the top and bottom walls of the tunnel in the region of the model, as well as downstream up to a distance of 45 cm. The pressures were measured with strain-gage pressure transducers; each transducer was calibrated before each tunnel run.

Wall shear-stress measurements were not made, but were inferred on the upper surfaces of the flat plate and flap by fitting the velocity data near the wall (obtained using pitot probes) to the law of the wall, which is valid in adverse pressure gradients except close to separation.

Flow-Field Measurements

Most flow-field measurements were made using a two-dimensional, two-color, laser Doppler velocimeter (LDV). Some measurements using conventional pitot and static probes were also carried out in certain regions of the flow. A schematic of the LDV set up is shown in figure 2. The two channels of the LDV were operated independently in two beam orientations: (1) beams aligned at ±45° (to the longitudinal tunnel axis), allowing measurement of U, V, $\langle uv\rangle$, and $\langle u^2 + v^2\rangle$; and (2) beams aligned along and perpendicular (0°, 90°) to the tunnel axis, thereby measuring U, V, $\langle u^2\rangle$, and $\langle v^2\rangle$. Most measurements, however, were carried out in the ±45° configuration; the 0°, 90° configuration was used only at selected stations where turbulence intensity measurements were desired. The optical arrangement used and the seeding employed are described in references 2 and 5. Details of data acquisition and data processing are given in appendix A.

The pitot probe that was used had a nearly rectangular mouth with a vertical opening of 0.005 cm and a total thickness of 0.025 cm. Two static pressure probes, one with an ellipsoidal and the other with a hemispherical nose, were used at different stations with appropriate calibration for each probe.

Flow Visualization

The flow was visualized using conventional Schlieren and shadowgraph techniques, and the surface flow on the flap was examined using an oil-flow technique to detect, for example, flow reversal and three-dimensional effects. A mixture of titanium dioxide, oleic acid, and vacuum pump oil was used.

Accuracy of Measured Data

The various error sources considered for the LDV measurements are as follows: optical, electronic, statistical, and positional.

Optical inaccuracies stem primarily from determination of the fringe spacing and precise orientation of the LDV fringe pattern with respect to the tunnel coordinate system. These errors are systematic and account for an error of about 1% in any individual velocity measurement.

Electronic inaccuracies for the system used are due in part to noise. This noise increases dramatically with glare from surface reflections. Error in velocity measurements caused by glare-induced noise were greatest within 0.25 cm of the surface. Such errors are random and serve to increase the measured turbulence intensities and reduce the repeatability of the mean-velocity measurements.

Statistical considerations in measuring a stochastic phenomenon such as turbulence include sample size and sample rate relative to integral time scales. The minimum sample size (n) used was 3,000 individual realizations. The contribution to the standard deviation of the mean velocity owing to finite sample size is given by (ref. 6):

$$\Delta u = (\langle u^2 \rangle / n)^{1/2}$$

Given that the maximum $\langle u^2 \rangle$ encountered in this study was less than 1300 m^2/sec^2, the maximum contribution to mean velocity error resulting from finite sample size is less than 1 m/sec.

The statistical issue of independence of individual velocity realizations influences the above estimate of mean velocity error owing to finite sample size. If the typical time interval between samples (LDV realizations) is less than twice the integral time scale of the turbulence then the individual samples are not statistically independent and the error cited above as being due to finite sample size is an underestimate. For the typical time interval between samples to be greater than twice the integral macroscale is not a guarantee of statistical independence of the samples, but it is a minimum condition. The LDV sample rate was typically between 100 to 1000 samples/sec for the shear-layer regions. Conservative estimates of the integral time scale for the flow field are all less than 0.5 msec.

Positional accuracy of the LDV optical carriage was an important consideration, particularly because of the small size of the separation bubble being studied.

Re-zeroing before each Y profile accounted for the backlash in the carriage unit used, thereby aiding in the repeatability of profiles. Even so, positioning accuracy and repeatability of the LDV optical carriage was ±0.04 cm in the Y direction.

Considering the various sources of error cited above, the mean velocity data are estimated to be accurate to within ±4% or ±4 m/sec, whichever is greater. Similarly, the turbulence quantities (<uv>, etc.) are deemed accurate to within ±8% or ±16 m^2/sec^2, whichever is greater. Because of glare and low seed level, the greatest inaccuracies occur in the separation region close to the body surface.

The velocity data determined from pitot and static measurements are estimated to be accurate to within ±3%.

The stated accuracy for the LDV mean-velocity measurements was verified through comparisons with velocity data calculated from pitot-static measurements. Shown in figure 3 is a comparison of wake mean-velocity profiles obtained by the two measurement techniques mentioned above. No attempt was made to adjust the LDV constants (e.g., beam angle) to force agreement with pitot-static measurements. Good agreement between the two profiles is seen and the differences in the region of minimum velocity are within the accuracy stated above.

Figures 4 and 5 show profiles of mean velocity and turbulent kinetic energy, respectively, measured at $X = -0.25$ cm, using the two different LDV beam orientations described above. Agreement of the two mean-velocity profiles is well within the accuracy cited earlier. The two kinetic-energy profiles also exhibit excellent agreement, except close to the surface ($Y \lesssim 0.5$) where intermittent flow reversal (to be discussed) and low seed levels occur.

Two-Dimensionality of the Flow Field

Two-dimensionality of the mean flow was validated, based on oil-flow patterns on the flap surface, observations of spanwise variations of certain flow quantities, and estimates of the two-dimensional boundary-layer momentum integral equation from the measured data.

During the initial phase of the experiments, surface oil-flow patterns on the flap showed slight asymmetric features about the centerline ($Z = 0$) of the tunnel; in particular, the size of the vortex-like patterns present in the two corners (often found on models spanning the tunnel sidewalls and with flow separation) were somewhat different. The central 50% of the span otherwise showed a nearly two-dimensional flow-reversal line. The asymmetry seen was thought to be a result of asymmetric sidewall boundary-layer separation. Measurements of spanwise variation of static pressure on the flap and wake pitot measurements (over the central 70% of the span) at a station 15 cm downstream of the trailing edge did not reveal any noticeable three-dimensional effects. Nevertheless, attempts were made to improve the surface-flow characteristics over a larger part of the span, using different passive devices. Vortex generators on the side walls, the flow guides suggested in reference 7, and vertical fences were all tried, but with limited success. Finally, there was considerable improvement when small vortex generators were located just upstream of the flat-plate/flap junction, as shown in figure 6. The vortex generators used were 4.4 cm long and 0.95 cm high; they were fixed on the flat plate at an angle of about 12° to the main flow direction. The leading edge of the generators did not protrude significantly beyond the sidewall boundary-layer thickness.

A representative oil-flow pattern on the upper surface of the flap at $M_n = 0.7$, with the vortex generators in the optimum position, is shown in figure 7. A thin film of oil mixture was painted on the initial part of the flap (for a distance of about 5 cm from the hinge-line), and small dots of oil were laid in the trailing-edge region where separation was expected. The thin sheet of oil flows downstream in the region of high wall-shear, and finally settles along a line where the boundary layer is separating. As may be seen in the photograph, the oil dots have moved in opposite directions on either side of the flow-reversal line, which is reasonably straight over a large part of the span. From the surface-flow pattern, the flow-reversal location, X_{fr}, is found to be at -2.0 ± 0.25 cm.

It is believed that the improvement seen is due to the control of the corner-separated flow under the influence of the vortex generators located upstream. All data to be presented here were obtained with the vortex generators in the optimum position.

Figure 8 shows a comparison of mean-velocity profiles in the wake along the centerline and at a spanwise location (Z = -6.35 cm); there is good agreement between the two. Surface static pressures on the flap (in the region of separation) also showed negligible variation over the central 80% of the span.

As a further check on the two-dimensionality of the mean flow, estimates of the different terms in the two-dimensional boundary-layer momentum integral equation have been made, using the measured data on the upper surface of the flap and in the wake.

For the boundary layer, the left-hand side (L.H.S.) and right-hand side (R.H.S.) of the integrated momentum equations are (see ref. 8)

$$\text{L.H.S.} = \frac{(\rho_e U_e^2 \Theta)_X}{(\rho_e U_e^2 \Theta)_{X_o}} - 1$$

$$\text{R.H.S.} = \int_o^X \frac{\delta^* \, dp}{(\rho_e U_e^2 \Theta)_{X_o}} + \int_o^X \frac{c_f}{2} \frac{\rho_e U_e^2 \, dx}{(\rho_e U_e^2 \Theta)_{X_o}}$$

The integral thickness parameters δ^* and Θ were estimated taking into account (in an approximate sense) the weak static-pressure gradients across the boundary layer, which arise as a result of streamline curvature. This issue is further discussed in appendix B.

The momentum-balance results for the flap upper surface are presented in figure 9(a). The agreement between the L.H.S and R.H.S. is good ahead of $X = -3$ cm, but differences arise and increase gradually toward the trailing edge (separated zone). This departure may be a result of neglecting the turbulent normal-stress terms, which often become important in separated flows (ref. 9). There is evidence (refs. 9, 10) that the contribution of the normal-stress term, $\partial\langle u^2\rangle/\partial X$, is largest compared with that of other terms that are neglected. From the measured data of $\langle u^2\rangle$, the above mentioned term was evaluated and included on the R.H.S. of the momentum integral equation. These are shown by the solid symbols in figure 9(a). The vertical bars represent the sensitivity of the results to a 5% uncertainty in Θ, an uncertainty that is typical in the measured data. The agreement between the L.H.S. and R.H.S. may be considered excellent all along the flap, with the inclusion of the turbulent normal-stress term.

Following the wake-closure, an asymmetric wake is formed, and it is necessary to determine the momentum balance considering the wake as a whole, since there is an interaction between the upper and lower sides of the wake. An approximate momentum integral equation derived within the boundary-layer approximation is used here (Viswanath unpublished). The wake results are shown in figure 9(b); the L.H.S. and R.H.S. again represent terms similar to those mentioned for the boundary layer, with the skin-friction term being zero. The agreement is considered excellent within the accuracy of the measured data.

As may be clear, only a small region in the vicinity of the trailing edge and wake-closure has been excluded from the momentum-balance calculations. The main reason for this is that large errors in the estimate occur in this region of rapid flow changes and these errors remain in the wake momentum-balance estimates if the calculations are carried through the trailing edge and into the wake.

Based on all these different observations and on momentum-balance calculations, mean-flow two-dimensionality is considered very good.

EXPERIMENTAL RESULTS

As stated earlier, the separated trailing-edge flow field at a Mach number of 0.7 and at a Reynolds number of 40×10^6 was selected for detailed documentation.

Model surface-pressure distributions (normalized by P_T) at the above chosen conditions are shown in figure 10. The model develops a circulation like an airfoil. The pressures on the lower surface beyond the forebody wedge region ($X > -70$ cm) is practically constant all the way up to the trailing-edge, as one would expect. On the upper surface, following weak pressure gradients on the flat-plate region, the pressure first decreases toward the flap hinge-line (in response to the sudden change in model curvature), and then increases on the flap. An expanded view of the flap pressures is presented in figure 11; the dashed lines indicate lower surface pressures. The pressure gradient relief (or pressure plateau) toward the trailing edge at $M_n = 0.7$ suggests flow separation (ref. 11). Separation was also confirmed by surface oil-flow observations (fig. 7). The data at $M_n = 0.5$ and 0.6 are also included in figure 11 to give an idea of the Mach number effects on pressure gradients on the flap and of the progressive formation of boundary layer separation.

The model centerline pressure distributions obtained with and without the vortex generators were essentially identical. Model and tunnel-wall pressures at all three Mach numbers are given in tables 1 and 2, respectively.

Flow Visualization

A spark shadowgraph of the flow field is shown in figure 12. The boundary layers and the wake can be distinguished from the background. Vortex like structures, rotating counterclockwise, are being shed at the trailing-edge on the lower surface.

Mean Flow Field

The mean-velocity data measured with a pitot tube above the upper surface of the flat plate at a location $X = -27.3$ cm are shown in figure 13 in law-of-the-wall coordinates. Good agreement may be seen, indicating a fully developed turbulent boundary layer ahead of the flap. The velocity data and integral thickness parameters are given in table 3. No such measurements could be carried out on the lower flat-plate surface, but the boundary layer ahead of the flap is likely to be turbulent and fully developed (like the upper surface) in view of the zero pressure gradient flow at high Reynolds number.

On the upper surface of the flap, pitot and LDV data were obtained at different streamwise stations. Pitot data were obtained at $X = -10.16$, -7.94, and -5.71 cm; LDV data were obtained in the region downstream. Static pressure across the boundary layer on the flap was measured only at $X = -7.94$ cm (fig. 14). The pressure variation relative to the value at the wall (P/P_{wall} vs Y) observed at $X = -7.94$ cm was also used at $X = -10.16$ and -5.71 cm for calculating velocity information from pitot data. Since the static pressure change across the boundary layer is small (about 5% of the wall value), the above assumption should be fairly realistic. All the mean and turbulence velocity data are presented normalized by a reference velocity (sonic speed), U_0, equal to 295.7 m/sec. This sonic speed is based on the static temperature corresponding to $T_T = 470°R$ and $M = 1$.

The mean-velocity profiles measured with a pitot tube above the flap upper surface, upstream of separation, are shown in figure 15. The deceleration of the entire profile (in particular, close to the wall) that results from continuous adverse pressure gradients is clearly seen. The velocity profiles measured by the LDV through separation and in the near-wake are presented in figure 16; an expanded view of the velocity profiles in the separated region is shown in figure 17. From the velocity profiles, accurate location of the separation could not be inferred because of lack of data very close to the wall. However, a careful observation of all measured velocity profiles in the vicinity of separation indicates that boundary-layer separation occurred in the range $-2.38 \leq X \leq -1.9$ cm. This location is consistent with the location at which flow reversal was inferred ($X_{fr} = -2.0 \pm 0.25$ cm) from surface-flow patterns. The height of the reversed flow (fig. 17) is small (≈ 0.20 cm) compared with the boundary-layer thickness. Wake-closure occurs downstream of the trailing edge at $X = 0.40$ cm. The mean-velocity data obtained from pitot-pressure measurements at $X = -10.16$, -7.94, and -5.71 cm are tabulated in table 4. The LDV measurements made downstream with the ±45° beam orientation are presented in table 5. Data of two profiles measured near the trailing-edge on the lower surface are given in table 6.

Static-pressure profiles in the near-wake (downstream of wake-closure) obtained with an ellipsoidal nose probe are displayed in figure 18. The probe was used with its axis parallel to the X-axis. The probe data have not been corrected to account for flow-inclination effects. Such corrections are likely to be important in a small region around $Y = 0$ at $X = 0.79$ and 1.91 cm, where the streamline inclinations are large. The probe had two static holes (180° apart) to minimize the incidence corrections for small flow angles.

Mean flow streamlines on the flap and in the near-wake, calculated using the mass-flow concept are shown in figure 19. The separation point S (as defined by X_{fr}), wake closure C, and the dividing streamlines are also shown in the figure.

The variation in boundary-layer integral thickness parameters above the upper surface of the flap and in the upper part of the wake over a short distance downstream of the trailing edge is shown in figure 20. The rapid increase in δ^* and H toward the trailing edge and their rapid initial decay in the near-wake may be clearly seen. At the surface-flow reversal location (X_{fr}), the integral parameters have the following values: Displacement thickness $\delta^* = 0.7$ cm; Momentum thickness $\Theta = 0.25$ cm; and Shape factor $H \simeq 2.8$. The manner in which δ^* and Θ were estimated, taking into account approximately the weak pressure variation across the boundary layer on the flap upper surface, is described in appendix B. In the near-wake, as an approximation, the flow was divided into two parts about the minimum velocity line, and the integral thickness parameters were estimated independently for the upper and lower flows in the boundary-layer sense. The values of these integral thickness parameters are presented in table 7.

The experimental wall shear-stress on the upper surface of the flap was inferred by fitting the velocity data (see fig. 21) near the wall (obtained using a pitot probe) to the law of the wall, which is valid in adverse-pressure-gradient flows (except close to separation), even with effects of convex curvature (refs. 12, 13). The pitot data were reduced with zero normal-pressure gradient across the boundary layer. This approximation does not affect the mean-velocity results near the wall; this is because the logarithmic region is limited to a very small physical dimension in high-Reynolds-number flows at these high-subsonic/transonic-Mach numbers (e.g., on a flat-plate boundary layer at $M = 0.8$, Y^+ of 500 corresponds to a height of about 0.04 cm), and there is evidence (fig. 14) that the pressure variation is negligible, at least in the inner third of the boundary-layer thickness. The c_f values were calculated using edge conditions as determined from measured surface pressure, tunnel total pressure, and tunnel total temperature along with isentropic flow relations. The inferred c_f values are given in table 8; they are estimated to be accurate within ±10%.

Turbulence Flow Field

Turbulent shear-stress and two-component, turbulent kinetic-energy profiles are shown in figures 22 and 23, respectively; these data are included in tables 5 and 6. Since the maximum density variation across the boundary layer is only about 10%, ρ is neglected in the definition of shear stress. In the separated zone, both turbulent shear stress and kinetic energy profiles show an increase in magnitude, particularly in the outer region.

Measurements of mean velocity and of streamwise and lateral turbulent intensities, obtained at selected streamwise stations using the 0°, 90° LDV beam orientation, are presented in table 9.

A feature relating to the time-dependent nature of the flow in the vicinity of separation is described next. One measure of the unsteady nature of separation is downstream intermittency (γ_p), defined as the fraction of the time the flow has a positive streamwise component. It was estimated from the measured data of streamwise velocity fluctuations (in the 0°, 90° beam configuration) in a manner similar to that of Simpson et al. (ref. 14). Measured U velocity distribution, rather than an assumed Gaussian distribution, was used. These results are shown in figure 24 for five different measurement stations. These show that the flow near the wall is separated on an intermittent basis, even upstream of the mean separation point ($X_{fr} \simeq -2$ cm).

Detailed analyses of the mean and turbulence flow-field data are reported in reference 4.

CONCLUDING REMARKS

Results from an experimental investigation of a small-scale, trailing-edge separated flow resulting from sustained adverse pressure gradients are presented. The experiment was made at a transonic Mach number and at a high Reynolds number representative of flight conditions. The measurements made are of sufficient detail and quality for use in the evaluation of turbulence models and calculation methods.

Since the experiment was carried out in a test section with solid upper and lower walls, it is important that wall effects be included in any prediction method attempting to calculate the entire flow field. Measured tunnel-wall pressures may be used as boundary conditions or for verifying any modeling of the tunnel walls that may be employed in the prediction method.

APPENDIX A

LDV DATA ACQUISITION AND REDUCTION

The laser Doppler velocimeter (LDV) used in the present study was a two-dimensional, two-color, counter-based system coupled by a high-speed digital interface to a 16-bit minicomputer.

The optical portion of the LDV, which has been reported in references 2 and 5, is an off-axis, forward-scatter system. The LDV was operated in a nonsimultaneous mode, for which the two channels of LDV are treated separately, and simultaneous measurements of velocity by the two orthogonal channels is not required. One feature of the system was the use of a 40-MHz Bragg cell in both of the LDV beam pairs, allowing measurements within the separation zone.

The two LDV counters used were built at Ames Research Center and are based on a pulse-stretching circuit. Whenever one of the counters measures a velocity, a 12-bit digital word is presented as output. Eleven of the 12 bits form an integer proportional to the time duration for eight fringe crossings. The twelfth bit indicates which of the two counters accomplished the measurement, and a TTL level pulse is generated indicating the occurrence of an LDV event. Since the system is being operated nonsimultaneously, the other counter need not have made a measurement.

Data acquisition of the above counter digital output was accomplished through a high-speed, 16-bit, parallel multiplexing interface into a PDP-11/34 minicomputer (Harrison and Brown, "A High Speed Interface for Analog and Digital Data Acquisition," report in preparation). When either of the two LDV counters presents an event pulse, indicating a measurement, the interface multiplexes the two LDV digital words into a single, 16-bit, parallel, direct-memory-access I/O port. Transfer was always of two digital words of LDV output, regardless of whether one or both channels of LDV realized a measurement. Thus, through the I/O port the LDV digital output was written two words at a time into an integer array. Typically, 3,096 to 10,240 word pairs were acquired, by the finish of data acquisition, at which time the entire array was written to digital magnetic tape for later processing.

The data stream stored on digital magnetic tape was subsequently analyzed by first forming a histogram (number of velocity realizations vs velocity) at each position for each channel. Pruning of each histogram (see fig. 25) to minimize the effects of noise was controlled visually. The histograms were then reanalyzed for the various statistics. Inclusion of an LDV digital word in the analysis was always conditioned on the presence of a set twelfth bit, indicating that the LDV data word represented valid new data in the data stream.

Each LDV counter actually measures the time interval for eight fringe crossings. Thus, channels A and B measure, respectively:

$$u_a = d_a s_a (b_a - 10000/dt_a)$$

$$u_b = d_b s_b (b_b - 10000/dt_b)$$

Where u is the velocity measured; d is the LDV fringe spacing; b is the calibration constant giving the Bragg cell frequency, as measured by each channel; s is the dimensionless calibration constant for the counter, and dt is the time for effectively 100 fringe crossings for each channel. The subscripts a and b refer to channels A and B, respectively. Time for eight fringe crossings is actually measured, but pulse stretching used in the counters stretches this time interval by a factor of 12.5. Calibration constants were checked daily after 30-min minimum warmup of the electronics. Small daily variations were noted; however, only four actual sets of calibration constants were used in this study.

The statistics for the two channels were analyzed separately. For the 0°, 90° orientation:

$$\langle U\rangle = \langle u_a\rangle$$

$$\langle V\rangle = \langle u_b\rangle$$

$$\langle u^2\rangle = \langle u_a{}^2\rangle$$

$$\langle v^2\rangle = \langle u_b{}^2\rangle$$

Since the histograms formed are an experimental measure of the velocity probability density function (Pdf), the u-component histogram was also analyzed for the fraction of measurements that were positive, γ_p. Figure 25 depicts γ_p as the ratio of the shaded area to the total area under the histogram. This quantity is considered relevant to separated flows. For fully attached flow without flow reversal, $\gamma_p = 1$.

For the ±45° orientation:

$$\langle u_a\rangle = \langle U + V\rangle/(2)^{1/2}$$

$$\langle u_b\rangle = \langle U - V\rangle/(2)^{1/2}$$

$$\langle u_a{}^2\rangle = \langle u^2 + 2uv + v^2\rangle/2$$

$$\langle u_b{}^2\rangle = \langle u^2 - 2uv + v^2\rangle/2$$

From the above averages the following mean quantities were formed:

$$\langle U\rangle = (\langle u_a\rangle + \langle u_b\rangle)(2)^{1/2}$$

$$\langle V\rangle = (\langle u_a\rangle - \langle u_b\rangle)(2)^{1/2}$$

$$\langle uv\rangle = \langle u_a{}^2\rangle - \langle u_b{}^2\rangle$$

$$\langle u^2 + v^2\rangle/2 = (\langle u_a{}^2\rangle + \langle u_b{}^2\rangle)/2$$

Analysis of γ_p in the ±45° model was not possible. Once an analysis was done, the basic statistics were written into a disk file for tabulation purposes and for plotting of profiles.

Further analysis for higher-order statistics is possible when operating in the simultaneous mode; however, such operation was delayed, pending minor modifications required to the optical system.

APPENDIX B

ESTIMATION OF BOUNDARY-LAYER INTEGRAL THICKNESS PARAMETERS

The following definitions (ref. 15) for displacement thickness δ^* and momentum thickness Θ, taking into account the pressure variation across the boundary layer, were used:

$$\delta^* = \int_o^\delta \left(1 - \frac{\rho U}{\rho_p U_p}\right) dy$$

$$\Theta = \int_o^\delta \frac{\rho U}{\rho_p U_p}\left(1 - \frac{U}{U_p}\right) dy$$

where ρ_p and U_p refer to the fictitious potential flow density and velocity, respectively; they are determined from the values of static pressure, free-stream total pressure, and free-stream total temperature used with isentropic-flow relations. The above definitions are frequently used on flows over curved surfaces (ref. 12).

On the upper surface of the flap, pitot data were obtained at $X = -10.16$, -7.94, and -5.71 cm; LDV data were obtained in the region downstream. The static-pressure variation across the boundary layer was measured only at $X = -7.94$ cm (see fig. 14); this variation was also used at $X = -10.16$ and -5.71 cm for reducing the pitot data. Since the static-pressure change across the layer is small, the above assumption should be fairly realistic. At stations where LDV was used, the pressure variations were estimated as follows. A best guess of Y_e was made based on near-constancy of turbulence quantities in the free stream. Using the values of the measured boundary-layer edge velocity and the free-stream total temperature, the free-stream static temperature was calculated, using the energy equation in which adiabatic flow is assumed. From the temperature information, Mach number and static pressure at the boundary-layer edge were determined from isentropic-flow relations. The static pressure was assumed to vary linearly between its value at the surface and at the boundary-layer edge.

The integral thickness parameters taking into account the pressure variation were generally higher; differences typically of about 5% and 10% were found in δ^* and Θ, respectively.

REFERENCES

1. Bradshaw, P.; Cantwell, B. J.; Ferziger, J. H.; and Kline, S. J.: Experimental Data Needs for Computational Fluid Dynamics — A Position Paper, 1980-81 AFOSR-HTTM-Stanford Conference on Complex Turbulent Flows: Comparison of Computation and Experiments, vol. I, Stanford, Calif., 1981.

2. Viswanath, P. R.; Cleary, J. W.; Seegmiller, H. L; and Horstman, C. C.: Trailing-Edge Flows at High Reynolds Number. AIAA Paper 79-1503, 1979.

3. Cleary, J. W.; Viswanath, P. R.; Horstman, C. C.; and Seegmiller, H. L.: Asymmetric Trailing-Edge Flows at High Reynolds Number. AIAA Paper 80-1396, 1980.

4. Viswanath, P. R.; and Brown, J. L.: Separated Trailing-Edge Flow at a Transonic Mach Number. AIAA Paper 82-0348, 1982.

5. Seegmiller, H. L.; Marvin, J. G.; and Levy, L. L.: Steady and Unsteady Transonic Flow. AIAA J., vol., 16, Dec. 1978, pp. 1262-1270.

6. Lumley, J. L: Stochastic Tools in Turbulence. Academic Press, New York, 1970.

7. Coles, D.; and Wadcock, A. J.: Flying Hot-Wire Study of Flow Past an NACA 4412 Airfoil at Maximum Lift. AIAA J., vol. 17, Apr. 1979, pp. 321-329.

8. Alber, I. E.; Bacon, J. W.; Masson, B. S.; and Collins, D. J.: An Experimental Investigation of Turbulent Transonic Viscous-Inviscid Interactions. AIAA Paper 71-565, June 1971.

9. Sovran, G.: On Predictions Criteria for Turbulent Separation. Proceedings of 1968 AFOSR-IFP-Conference on Computation of Turbulent Boundary Layers, vol. 1, Stanford U., Stanford, Calif., 1968.

10. Bidwell, J. M.: Application of the Von-Karman Momentum Theorem to Turbulent Boundary Layers. NACA TN-2571, 1951.

11. Cebeci, T.; Mosinskis, G. J.; and Smith, A. M. O.: Calculation of Separation Points in Incompressible Turbulent Flows. J. Aircraft, Vol. 9, 1972, pp. 618-624.

12. So, R. M. C.; and Mellor, G. L.: An Experimental Investigation of Turbulent Boundary Layers along Curved Surfaces. NASA CR-1940, 1972.

13. Lakshmana Gowda, B. H.; and Aswathnarayana, P. A.: An Experimental Investigation of Separating Flow on a Convex Surface. Appl. Sci. Res., vol. 36, 1980, pp. 271-288.

14. Simpson, R. L.; Strickland, J. H.; and Barr, P. W.: Features of a Separating Turbulent Boundary Layer in the Vicinity of Separation. J. Fluid Mech., vol. 79, 1977, pp. 552-594.

15. Cook, P. J.; McDonald, M. A.; and Firmin, M. C. P.: Aerofoil RAE 2822-Pressure Distributions and Boundary Layer and Wake Measurements. AGARD-AR-138, May 1979.

TABLE 1.- MODEL STATIC-PRESSURE DISTRIBUTIONS

Upper Surface				Lower Surface			
X/L	P/PT	X/L	P/PT	X/L	P/PT	X/L	P/PT
$M_n = 0.5$; $Re_L = 31 \times 10^6$							
-.941	.793	-.168	.757	-.941	.860	-.168	.841
-.876	.797	-.146	.748	-.876	.856	-.146	.845
-.813	.785	-.134	.734	-.813	.849	-.128	.842
-.780	.784	-.121	.731	-.780	.846	-.108	.844
-.748	.773	-.108	.732	-.748	.840	-.088	.842
-.711	.774	-.094	.742	-.711	.843	-.068	.844
-.680	.773	-.081	.752	-.680	.844	-.048	.842
-.616	.777	-.068	.767	-.616	.842	-.028	.842
-.552	.773	-.054	.782	-.552	.842	-.015	.841
-.488	.770	-.041	.800	-.488	.844	-.003	.840
-.424	.776	-.031	.820	-.424	.843		
-.361	.774	-.021	.825	-.361	.843		
-.296	.771	-.015	.837	-.296	.842		
-.233	.768	-.008	.839	-.233	.840		
-.201	.761	-.003	.840	-.201	.840		
$M_n = 0.6$; $Re_L = 36 \times 10^6$							
-.941	.717	-.168	.650	-.941	.804	-.168	.775
-.876	.719	-.146	.640	-.876	.799	-.146	.780
-.813	.701	-.134	.614	-.813	.789	-.128	.775
-.780	.697	-.121	.612	-.780	.785	-.108	.777
-.748	.680	-.108	.617	-.748	.776	-.088	.775
-.711	.682	-.094	.633	-.711	.779	-.068	.778
-.680	.680	-.081	.653	-.680	.781	-.048	.776
-.616	.683	-.068	.676	-.616	.778	-.028	.775
-.552	.678	-.054	.701	-.552	.779	-.015	.773
-.488	.674	-.041	.725	-.488	.782	-.003	.769
-.424	.677	-.031	.750	-.424	.778		
-.361	.674	-.021	.754	-.361	.778		
-.296	.681	-.015	.765	-.296	.777		
-.233	.664	-.008	.767	-.233	.776		
-.201	.656	-.003	.767	-.201	.778		
$M_n = 0.7$; $Re_L = 40 \times 10^6$							
-.941	.687	-.168	.573	-.941	.774	-.168	.742
-.876	.683	-.146	.546	-.876	.767	-.128	.737
-.813	.661	-.134	.514	-.813	.757	-.108	.740
-.780	.654	-.121	.521	-.780	.753	-.088	.740
-.748	.626	-.108	.540	-.748	.741	-.068	.743
-.711	.638	-.094	.567	-.711	.745	-.048	.742
-.680	.634	-.081	.600	-.680	.746	-.028	.740
-.616	.634	-.068	.633	-.616	.742	-.015	.732
-.552	.630	-.054	.664	-.552	.744	-.003	.726
-.488	.624	-.041	.691	-.488	.747		
-.424	.621	-.031	.706	-.424	.744		
-.361	.616	-.021	.712	-.361	.744		
-.296	.659	-.015	.717	-.296	.741		
-.233	.600	-.008	.720	-.233	.743		
-.201	.591	-.003	.720	-.201	.743		

TABLE 2.- TUNNEL-WALL STATIC PRESSURE-DISTRIBUTIONS

M_n = 0.5; Re_L = 31 × 10^6				M_n = 0.6; Re_L = 36 × 10^6				M_n = 0.7; Re_L = 40 × 10^6			
Upper wall		Lower wall		Upper wall		Lower wall		Upper wall		Lower wall	
X/L	P/PT	X/L	P/PT	X/L	P/PT	X/L	P/PT	X/L	P/PT	X/L	P/PT
-1.013	.820	-1.013	.856	-1.013	.754	-1.013	.804	-1.013	.733	-1.013	.781
-.960	.815	-.960	.858	-.960	.746	-.960	.805	-.960	.718	-.960	.782
-.853	.798	-.853	.854	-.853	.718	-.853	.796	-.853	.684	-.853	.770
-.747		-.747	.848	-.747		-.747	.789	-.747		-.747	.760
-.640	.776	-.640	.843	-.640	.683	-.640	.784	-.640	.640	-.640	.754
-.534	.771	-.534	.844	-.534	.675	-.534	.782	-.534	.628	-.534	.751
-.427	.771	-.427	.841	-.427	.672	-.427	.777	-.427	.622	-.427	.747
-.321	.768	-.321	.842	-.321	.668	-.321	.777	-.321	.614	-.321	.747
-.214	.767	-.214	.842	-.214	.666	-.214	.775	-.214	.621	-.214	.745
-.108	.780	-.108	.841	-.108	.689	-.108	.776	-.108	.636	-.108	.743
-.001	.806	-.001	.839	-.001	.729	-.001	.774	-.001	.690	-.001	.743
.105	.820	.105	.835	.105	.751	.105	.771	.105	.718	.105	.741
.212	.825	.212	.832	.212	.759	.212	.766	.212	.727	.212	.738
.318	.826	.318	.828	.318	.759	.318	.762	.318	.728	.318	.733
.425	.826	.425		.425	.759	.425		.425	.728	.425	.731
.531	.824	.531	.816	.531	.755	.531	.752	.531	.723	.531	.728

TABLE 3.- FLAT-PLATE BOUNDARY-LAYER PROFILE

[X = -27.3 cm; M_n = 0.7; Re_L = 40 × 10^6]

Y, cm	U/U_o	Y, cm	U/U_o
0.0000	0.000	.2489	.756
.0127	.513	.2718	.762
.0229	.551	.2946	.768
.0305	.575	.3150	.773
.0406	.600	.3353	.779
.0533	.628	.3556	.783
.0635	.647	.4572	.805
.0737	.660	.5613	.823
.0838	.672	.6655	.838
.0940	.682	.7671	.851
.1041	.689	.8738	.861
.1143	.697	.9754	.869
.1346	.710	1.0770	.873
.1448	.716	1.1786	.880
.1651	.725	1.2852	.885
.1854	.734	1.3868	.889
.2057	.742	1.4884	.890
.2286	.749	1.6916	.891

Note: Displacement thickness = 0.15 cm;
momentum thickness = 0.09 cm;
skin friction coefficient = 0.0019.

TABLE 4.- BOUNDARY-LAYER PROFILES

[$M_n = 0.7$; $Re_L = 40 \times 10^6$]

X = -10.16 cm		X = -7.94 cm		X = -5.71 cm	
Y, cm	U/U_o	Y, cm	U/U_o	Y, cm	U/U_o
0.0000	0.000	0.0000	0.000	0.0000	0.000
.0127	.646	.0127	.384	.0127	.254
.0254	.670	.0229	.407	.0330	.299
.0356	.691	.0330	.434	.0432	.326
.0457	.713	.0432	.477	.0533	.348
.0559	.729	.0533	.506	.0660	.371
.0660	.744	.0635	.533	.0762	.384
.0787	.758	.0762	.554	.0864	.399
.0889	.771	.0864	.574	.0965	.418
.0991	.786	.0965	.593	.1067	.432
.1092	.792	.1067	.610	.1168	.442
.1219	.801	.1168	.625	.1270	.457
.1321	.808	.1270	.640	.1397	.472
.1524	.818	.1372	.652	.1600	.495
.1727	.826	.1575	.672	.1829	.522
.1956	.835	.1803	.694	.2032	.544
.2159	.841	.2007	.708	.2235	.563
.2362	.848	.2235	.719	.2438	.579
.2591	.855	.2438	.734	.2667	.598
.2794	.857	.2642	.740	.2870	.610
.2997	.861	.2845	.749	.3099	.621
.3226	.864	.3048	.755	.3302	.632
.3429	.868	.3302	.761	.3505	.639
.3632	.872	.3505	.766	.3734	.648
.4699	.888	.4547	.790	.4775	.679
.5766	.898	.5588	.803	.5842	.700
.6833	.911	.6655	.818	.6909	.715
.7874	.918	.7722	.832	.7950	.728
.8941	.927	.9830	.846	.8992	.739
1.1049	.939	1.1963	.856	1.1125	.759
1.3157	.946	1.4072	.865	1.3208	.778
1.5291	.952	1.6180	.868	1.5342	.785
1.6459	.953	1.8288	.868	1.7475	.790
1.8593	.951	2.0422	.868	1.9583	.787
2.0701	.949	2.2530	.866	2.1717	.784
2.2809	.948			2.3825	.781
				2.5908	.776

TABLE 5.- BOUNDARY-LAYER AND WAKE PROFILES: MEAN AND TURBULENCE DATA

$[M_n = 0.7;\ Re_L = 40 \times 10^6]$

X = -2.86 cm				X = -2.38 cm			
Y, cm	U/U_o	$-\langle uv\rangle/U_o^2$	$\langle u^2+v^2\rangle/2U_o^2$	Y, cm	U/U_o	$-\langle uv\rangle/U_o^2$	$\langle u^2+v^2\rangle/2U_o^2$
5.1181	8.55E-01	-2.03E-04	3.10E-04	5.1181	8.33E-01	-3.23E-04	4.44E-04
4.6101	8.55E-01	-2.19E-04	3.32E-04	4.6101	8.33E-01	-3.15E-04	4.37E-04
4.1021	8.54E-01	-2.02E-04	3.10E-04	4.1021	8.34E-01	-2.94E-04	4.27E-04
3.5941	8.49E-01	-2.12E-04	3.54E-04	3.5941	8.31E-01	-2.14E-04	3.59E-04
3.0861	8.38E-01	-2.14E-04	3.81E-04	3.0861	8.23E-01	-1.44E-04	3.09E-04
2.5781	8.16E-01	-1.70E-04	6.53E-04	2.5781	8.12E-01	-7.46E-05	3.03E-04
2.3241	8.06E-01	-1.87E-04	5.73E-04	2.3241	7.96E-01	-4.08E-05	3.11E-04
2.0701	7.96E-01	-1.22E-04	6.44E-04	2.0701	7.81E-01	7.61E-05	4.57E-04
1.8161	7.78E-01	-3.28E-05	7.03E-04	1.9431	7.74E-01	1.18E-04	5.25E-04
1.6891	7.67E-01	3.95E-05	7.79E-04	1.8161	7.61E-01	1.70E-04	5.92E-04
1.5621	7.56E-01	1.86E-04	9.37E-04	1.6891	7.53E-01	2.33E-04	7.18E-04
1.3081	7.20E-01	2.66E-04	1.08E-03	1.5621	7.39E-01	2.82E-04	8.19E-04
1.1811	7.01E-01	3.49E-04	1.27E-03	1.4351	7.21E-01	3.43E-04	9.96E-04
1.0541	6.79E-01	4.90E-04	1.48E-03	1.3081	7.04E-01	4.52E-04	1.20E-03
0.9271	6.48E-01	6.41E-04	1.61E-03	1.1811	6.78E-01	5.71E-04	1.36E-03
0.8001	6.09E-01	9.41E-04	2.11E-03	1.0541	6.53E-01	7.04E-04	1.54E-03
0.6731	5.58E-01	1.46E-03	2.89E-03	0.9271	6.19E-01	9.47E-04	1.90E-03
0.5969	5.16E-01	2.14E-03	3.88E-03	0.8001	5.73E-01	1.44E-03	2.67E-03
0.5461	4.80E-01	2.44E-03	4.53E-03	0.6731	5.06E-01	2.26E-03	4.06E-03
0.4953	4.37E-01	2.87E-03	5.43E-03	0.5969	4.53E-01	2.64E-03	4.77E-03
0.4445	3.86E-01	3.59E-03	6.26E-03	0.5461	4.12E-01	3.02E-03	5.60E-03
0.3683	3.31E-01	3.44E-03	6.14E-03	0.4953	3.79E-01	3.17E-03	5.81E-03
0.2921	2.57E-01	3.06E-03	6.15E-03	0.4191	3.10E-01	3.41E-03	6.28E-03
0.1905	1.93E-01	2.10E-03	4.68E-03	0.3429	2.45E-01	3.25E-03	6.16E-03
0.1651	1.73E-01	2.24E-03	4.98E-03	0.2921	2.11E-01	2.73E-03	5.60E-03
0.1397	1.45E-01	1.77E-03	4.35E-03	0.2667	1.95E-01	2.82E-03	5.60E-03
				0.2159	1.56E-01	2.68E-03	5.54E-03
				0.1905	1.43E-01	2.51E-03	5.33E-03
				0.1651	1.27E-01	2.33E-03	5.21E-03
				0.1397	1.09E-01	2.22E-03	5.08E-03

TABLE 5.- CONTINUED

X = -1.270 cm				X = -0.25 cm			
Y, cm	U/U_o	$-\langle uv\rangle/U_o^2$	$\langle u^2+v^2\rangle/2U_o^2$	Y, cm	U/U_o	$-\langle uv\rangle/U_o^2$	$\langle u^2+v^2\rangle/2U_o^2$
5.1308	8.20E-01	-3.15E-04	5.08E-04	5.1054	8.13E-01	-2.29E-04	4.60E-04
4.4958	8.17E-01	-2.58E-04	4.70E-04	4.5974	8.07E-01	-1.64E-04	4.10E-04
4.1148	8.17E-01	-1.99E-04	4.27E-04	4.0894	7.97E-01	-1.00E-04	3.34E-04
3.8608	8.03E-01	-1.92E-04	3.78E-04	3.5814	7.86E-01	-4.87E-05	2.86E-04
3.6068	8.05E-01	-1.41E-04	3.71E-04	3.2004	7.80E-01	1.77E-06	2.68E-04
3.3528	7.92E-01	-1.20E-04	3.52E-04	2.8194	7.61E-01	5.98E-05	2.68E-04
3.0988	7.92E-01	-6.07E-05	3.40E-04	2.5654	7.49E-01	1.14E-04	3.42E-04
2.8448	7.77E-01	-3.99E-05	2.94E-04	2.3114	7.32E-01	2.17E-04	5.05E-04
2.5908	7.67E-01	2.75E-05	3.27E-04	2.0574	7.09E-01	3.30E-04	7.37E-04
2.3368	7.56E-01	6.18E-05	3.69E-04	1.8034	6.75E-01	4.94E-04	1.06E-03
2.0828	7.38E-01	1.42E-04	5.02E-04	1.5494	6.32E-01	8.01E-04	1.53E-03
1.8288	7.12E-01	2.36E-04	7.17E-04	1.2954	5.63E-01	1.46E-03	2.67E-03
1.7780	7.12E-01	2.91E-04	6.93E-04	1.1684	5.08E-01	2.30E-03	4.16E-03
1.5748	6.89E-01	6.33E-04	1.35E-03	1.0414	4.40E-01	3.15E-03	5.78E-03
1.4478	6.66E-01	4.88E-04	1.09E-03	0.9144	3.65E-01	3.63E-03	6.65E-03
1.3208	6.42E-01	6.62E-04	1.32E-03	0.7874	2.85E-01	3.95E-03	7.25E-03
1.2700	6.30E-01	7.19E-04	1.52E-03	0.6604	2.13E-01	3.50E-03	6.59E-03
1.1938	6.13E-01	9.58E-04	1.79E-03	0.5334	1.64E-01	2.44E-03	5.40E-03
1.0668	5.67E-01	1.31E-03	2.47E-03	0.4572	1.32E-01	2.55E-03	5.25E-03
1.0160	5.55E-01	1.63E-03	3.03E-03	0.3810	9.35E-02	2.40E-03	4.94E-03
0.9398	5.28E-01	1.84E-03	3.35E-03	0.3302	6.25E-02	2.21E-03	4.68E-03
0.8128	4.61E-01	2.57E-03	4.79E-03	0.2794	4.96E-02	2.25E-03	4.47E-03
0.7620	4.13E-01	2.98E-03	5.57E-03	0.1778	6.41E-03	1.87E-03	3.51E-03
0.6858	3.35E-01	3.37E-03	6.34E-03	0.1524	-4.19E-03	1.64E-03	3.15E-03
0.5588	2.66E-01	3.30E-03	6.44E-03	0.1270	-1.42E-02	1.38E-03	2.77E-03
0.5080	2.37E-01	2.95E-03	6.09E-03				
0.4318	1.92E-01	2.95E-03	5.96E-03				
0.3556	1.46E-01	2.43E-03	5.36E-03				
0.3302	1.27E-01	2.35E-03	5.21E-03				
0.3048	1.25E-01	2.39E-03	5.17E-03				
0.2540	9.04E-02	2.70E-03	5.16E-03				
0.2286	7.45E-02	2.39E-03	4.85E-03				
0.2032	4.50E-02	2.25E-03	4.47E-03				
0.1778	2.38E-02	2.22E-03	4.43E-03				

TABLE 5. CONTINUED

X = 0.40 cm				X = 0.64 cm			
Y, cm	U/U_o	$-\langle uv\rangle/U_o^2$	$\langle u^2+v^2\rangle/2U_o^2$	Y, cm	U/U_o	$-\langle uv\rangle/U_o^2$	$\langle u^2+v^2\rangle/2U_o^2$
5.0800	8.09E-01	-1.89E-04	4.71E-04	5.0800	8.08E-01	-1.73E-04	3.32E-04
4.4450	8.01E-01	-9.03E-05	3.75E-04	4.4450	7.99E-01	-1.13E-04	2.96E-04
3.8100	7.88E-01	-2.25E-05	3.25E-04	3.8100	7.85E-01	-6.84E-05	2.62E-04
3.1750	7.68E-01	4.30E-05	3.18E-04	3.1750	7.61E-01	3.23E-06	3.53E-04
2.5400	7.40E-01	2.05E-04	4.65E-04	2.5400	7.32E-01	9.99E-05	4.58E-04
2.2860	7.22E-01	2.41E-04	5.53E-04	2.0320	6.87E-01	2.79E-04	8.08E-04
2.0320	6.94E-01	3.38E-04	7.65E-04	1.7780	6.55E-01	4.61E-04	1.06E-03
1.7780	6.62E-01	5.52E-04	1.09E-03	1.5240	6.05E-01	9.19E-04	1.78E-03
1.5240	6.13E-01	9.79E-04	1.77E-03	1.3970	5.76E-01	1.19E-03	2.38E-03
1.3970	5.75E-01	1.35E-03	2.59E-03	1.2700	5.29E-01	1.89E-03	3.51E-03
1.2700	5.32E-01	1.79E-03	3.45E-03	1.1430	4.79E-01	2.21E-03	4.52E-03
1.1430	4.80E-01	2.42E-03	4.67E-03	1.0160	4.20E-01	3.00E-03	6.00E-03
1.0160	4.19E-01	3.08E-03	6.31E-03	0.8890	3.47E-01	3.85E-03	7.31E-03
0.8890	3.59E-01	3.61E-03	7.04E-03	0.7620	2.79E-01	3.68E-03	7.39E-03
0.7620	2.78E-01	3.46E-03	6.74E-03	0.6350	2.14E-01	3.51E-03	7.32E-03
0.6350	2.09E-01	2.88E-03	6.53E-03	0.5080	1.43E-01	2.86E-03	6.76E-03
0.5080	1.51E-01	2.57E-03	6.36E-03	0.4064	8.38E-02	2.09E-03	5.99E-03
0.3810	8.42E-02	2.09E-03	5.78E-03	0.3302	5.81E-02	1.63E-03	5.70E-03
0.3048	5.79E-02	1.81E-03	5.57E-03	0.2540	5.43E-02	-7.41E-04	5.67E-03
0.2540	1.04E-02	9.90E-04	4.44E-03	0.2032	7.44E-02	-2.47E-03	6.02E-03
0.2286	1.68E-02	9.10E-04	4.68E-03	0.1270	1.62E-01	-5.94E-03	8.50E-03
0.1524	6.12E-03	-4.00E-04	3.81E-03	0.0508	3.98E-01	-2.82E-03	6.45E-03
0.1270	1.41E-02	-1.21E-03	3.99E-03	0.0000	4.73E-01	-2.05E-03	4.38E-03
0.0762	9.44E-02	-3.81E-03	5.79E-03	-0.0508	5.20E-01	-1.20E-03	2.58E-03
0.0000	3.82E-01	-3.08E-03	6.42E-03	-0.1270	5.50E-01	-5.12E-04	1.45E-03
-0.1270	5.45E-01	-4.08E-04	1.44E-03	-0.2540	5.78E-01	-4.16E-04	1.12E-03
-0.2540	5.74E-01	-4.01E-04	1.24E-03	-0.3810	6.03E-01	-2.87E-04	9.55E-04
-0.3810	5.98E-01	-3.83E-04	1.00E-03	-0.5080	6.31E-01	-1.52E-04	6.91E-04
-0.5080	6.22E-01	-3.11E-04	8.49E-04	-0.6350	6.50E-01	-8.86E-05	5.40E-04
-0.6350	6.45E-01	-2.33E-04	6.59E-04	-1.0160	6.84E-01	-9.57E-05	2.04E-04
-0.7620	6.61E-01	-1.88E-04	5.61E-04	-1.1430	6.89E-01	-6.85E-05	1.69E-04
-1.0160	6.79E-01	-4.19E-06	1.99E-04	-1.5240	6.95E-01	-4.44E-05	1.29E-04
-1.2700	6.88E-01	2.30E-05	1.11E-04	-2.5400	6.98E-01	-4.00E-05	1.31E-04
-1.5240	6.90E-01	2.22E-05	9.95E-05	-5.0800	6.86E-01	-1.34E-05	6.01E-05
-2.0320	6.90E-01	2.42E-05	1.05E-04				
-2.5400	6.91E-01	2.17E-05	1.07E-04				
-3.0480	6.90E-01	2.10E-05	9.82E-05				
-3.5560	6.90E-01	1.84E-05	9.50E-05				
-4.0640	6.90E-01	1.76E-05	9.55E-05				
-4.5720	6.91E-01	1.85E-05	9.27E-05				
-5.0800	6.92E-01	2.26E-05	9.98E-05				

TABLE 5.- CONTINUED

X = 1.91 cm				X = 5.080 cm			
Y, cm	U/U_o	$-\langle uv\rangle/U_o^2$	$\langle u^2+v^2\rangle/2U_o^2$	Y, cm	U/U_o	$-\langle uv\rangle/U_o^2$	$\langle u^2+v^2\rangle/2U_o^2$
5.0800	7.93E-01	-9.49E-05	5.43E-04	5.5880	7.69E-01	-6.64E-05	5.52E-04
4.4450	7.83E-01	-3.73E-05	4.37E-04	5.0800	7.66E-01	-2.63E-05	4.79E-04
3.8100	7.69E-01	4.48E-06	3.36E-04	4.4450	7.55E-01	3.80E-05	4.01E-04
3.1750	7.50E-01	6.81E-05	2.64E-04	3.8100	7.42E-01	7.11E-05	2.69E-04
2.5400	7.28E-01	1.58E-04	3.39E-04	3.1750	7.28E-01	8.42E-05	2.13E-04
2.2860	7.13E-01	2.03E-04	4.18E-04	2.5400	7.09E-01	1.16E-04	2.20E-04
2.0320	6.98E-01	2.93E-04	6.00E-04	2.2860	7.00E-01	1.70E-04	2.86E-04
1.7780	6.66E-01	4.27E-04	8.74E-04	2.0320	6.86E-01	2.57E-04	4.31E-04
1.6510	6.49E-01	5.64E-04	1.08E-03	1.7780	6.64E-01	4.72E-04	7.66E-04
1.5240	6.23E-01	9.53E-04	1.69E-03	1.6510	6.51E-01	6.07E-04	9.96E-04
1.3970	6.01E-01	1.03E-03	1.91E-03	1.5240	6.31E-01	8.58E-04	1.41E-03
1.2700	5.61E-01	1.44E-03	2.89E-03	1.3970	6.09E-01	1.19E-03	2.00E-03
1.1430	5.26E-01	1.89E-03	3.94E-03	1.2700	5.89E-01	1.41E-03	2.50E-03
1.0160	4.67E-01	2.57E-03	5.46E-03	1.1430	5.59E-01	1.75E-03	3.35E-03
0.8890	4.20E-01	2.81E-03	6.15E-03	1.0160	5.30E-01	2.08E-03	3.98E-03
0.7620	3.49E-01	3.20E-03	6.85E-03	0.8890	4.89E-01	2.58E-03	4.85E-03
0.7112	3.27E-01	3.34E-03	7.29E-03	0.7620	4.67E-01	2.68E-03	5.07E-03
0.6350	2.90E-01	3.60E-03	7.33E-03	0.6350	4.23E-01	2.76E-03	5.17E-03
0.5588	2.55E-01	3.54E-03	7.18E-03	0.5080	3.94E-01	2.42E-03	4.94E-03
0.5080	2.29E-01	3.32E-03	7.00E-03	0.4318	3.78E-01	1.84E-03	4.77E-03
0.4572	2.08E-01	2.86E-03	6.65E-03	0.3556	3.69E-01	8.98E-04	4.72E-03
0.3810	1.92E-01	1.35E-03	6.00E-03	0.2794	3.65E-01	-3.52E-04	4.61E-03
0.3302	1.86E-01	-2.18E-05	6.17E-03	0.2032	3.70E-01	-1.19E-03	4.84E-03
0.2540	1.97E-01	-2.69E-03	6.79E-03	0.1270	3.88E-01	-2.51E-03	5.49E-03
0.2032	2.24E-01	-4.54E-03	7.89E-03	0.0000	4.19E-01	-3.46E-03	5.81E-03
0.1270	2.93E-01	-6.52E-03	9.36E-03	-0.1270	4.74E-01	-3.64E-03	5.62E-03
0.0000	4.14E-01	-4.57E-03	7.24E-03	-0.2540	5.21E-01	-3.24E-03	4.87E-03
-0.1270	5.02E-01	-2.73E-03	4.54E-03	-0.3810	5.65E-01	-1.92E-03	3.21E-03
-0.2540	5.52E-01	-1.50E-03	2.59E-03	-0.5080	6.01E-01	-1.26E-03	2.16E-03
-0.3810	5.87E-01	-7.07E-04	1.44E-03	-0.6350	6.28E-01	-7.83E-04	1.44E-03
-0.5080	6.09E-01	-3.48E-04	9.76E-04	-0.7620	6.50E-01	-3.93E-04	8.66E-04
-0.6350	6.30E-01	-2.17E-04	7.96E-04	-1.0160	6.78E-01	-4.45E-05	2.47E-04
-0.7620	6.49E-01	-1.29E-04	5.49E-04	-1.2700	6.87E-01	1.58E-05	1.03E-04
-0.8890	6.67E-01	-3.94E-05	3.42E-04	-1.5240	6.90E-01	2.47E-05	7.92E-05
-1.0160	6.75E-01	-5.29E-06	2.42E-04	-2.0320	6.90E-01	2.08E-05	6.99E-05
-1.2700	6.85E-01	2.04E-05	1.10E-04	-2.5400	6.90E-01	1.98E-05	6.66E-05
-1.5240	6.87E-01	1.88E-05	9.50E-05	-3.0480	6.90E-01	1.98E-05	6.74E-05
-1.7780	6.87E-01	1.92E-05	9.07E-05	-3.5560	6.91E-01	2.34E-05	6.71E-05
-2.0320	6.87E-01	2.02E-05	9.09E-05	-4.0640	6.91E-01	2.18E-05	6.33E-05
-2.5400	6.87E-01	1.76E-05	9.30E-05	-4.5720	6.92E-01	2.17E-05	6.18E-05
-3.1750	6.87E-01	2.28E-05	9.19E-05	-5.0800	6.94E-01	2.23E-05	6.20E-05
-3.8100	6.87E-01	2.27E-05	9.24E-05				
-4.4450	6.87E-01	2.08E-05	7.84E-05				
-5.0800	6.89E-01	2.55E-05	8.96E-05				

TABLE 5.- CONCLUDED

X = 7.620 cm				X = 12.07 cm			
Y, cm	U/U_o	$-\langle uv\rangle/U_o^2$	$\langle u^2 + v^2\rangle/2U_o^2$	Y, cm	U/U_o	$-\langle uv\rangle/U_o^2$	$\langle u^2 + v^2\rangle/2U_o^2$
5.0800	7.53E-01	-1.21E-06	4.42E-04	5.5880	7.42E-01	5.58E-05	4.02E-04
4.4450	7.45E-01	4.02E-05	3.34E-04	5.0800	7.40E-01	8.39E-05	3.52E-04
3.8100	7.33E-01	6.35E-05	2.43E-04	4.5720	7.36E-01	9.92E-05	3.11E-04
3.1750	7.20E-01	8.75E-05	2.10E-04	4.0640	7.32E-01	1.04E-04	2.36E-04
2.5400	7.05E-01	1.13E-04	2.21E-04	3.5560	7.22E-01	9.56E-05	1.76E-04
2.2869	6.97E-01	1.58E-04	2.80E-04	3.0480	7.14E-01	9.02E-05	1.46E-04
2.0320	6.85E-01	2.86E-04	4.61E-04	2.5400	7.07E-01	1.01E-04	1.62E-04
1.7780	6.68E-01	5.62E-04	8.80E-04	2.2860	7.01E-01	1.38E-04	2.30E-04
1.5240	6.42E-01	8.79E-04	1.47E-03	2.0320	6.92E-01	2.82E-04	4.19E-04
1.3970	6.24E-01	1.10E-03	1.84E-03	1.7780	6.82E-01	5.30E-04	7.29E-04
1.2700	6.03E-01	1.40E-03	2.39E-03	1.6510	6.71E-01	6.61E-04	9.84E-04
1.1430	5.81E-01	1.73E-03	2.95E-03	1.5240	6.60E-01	7.57E-04	1.19E-03
1.0160	5.49E-01	2.03E-03	3.49E-03	1.3970	6.47E-01	9.33E-04	1.52E-03
0.8890	5.25E-01	2.29E-03	4.29E-03	1.2700	6.34E-01	1.12E-03	1.92E-03
0.7620	4.94E-01	2.49E-03	4.48E-03	1.1430	6.10E-01	1.37E-03	2.38E-03
0.6350	4.73E-01	2.26E-03	4.18E-03	1.0160	6.06E-01	1.43E-03	2.52E-03
0.5080	4.50E-01	1.91E-03	3.96E-03	0.8890	5.73E-01	1.65E-03	3.02E-03
0.4064	4.34E-01	1.43E-03	3.92E-03	0.7620	5.63E-01	1.81E-03	3.43E-03
0.3048	4.29E-01	6.02E-04	4.05E-03	0.6350	5.35E-01	1.75E-03	3.30E-03
0.2032	4.20E-01	-2.33E-04	4.40E-03	0.5080	5.13E-01	1.52E-03	3.24E-03
0.1016	4.36E-01	-1.17E-03	4.18E-03	0.3810	5.05E-01	1.30E-03	3.28E-03
0.0000	4.50E-01	-2.01E-03	4.48E-03	0.2540	4.93E-01	7.91E-04	3.18E-03
-0.1270	4.79E-01	-2.77E-03	4.75E-03	0.1270	4.90E-01	1.14E-04	3.02E-03
-0.2540	5.15E-01	-2.86E-03	4.64E-03	0.0000	4.92E-01	-4.42E-04	3.13E-03
-0.3810	5.54E-01	-2.45E-03	4.01E-03	-0.1270	4.99E-01	-1.03E-03	3.28E-03
-0.5080	5.86E-01	-1.72E-03	3.00E-03	-0.2540	5.14E-01	-1.59E-03	3.51E-03
-0.6350	6.21E-01	-1.14E-03	2.01E-03	-0.3810	5.36E-01	-2.04E-03	3.63E-03
-0.7620	6.43E-01	-7.78E-04	1.42E-03	-0.5080	5.60E-01	-2.13E-03	3.59E-03
-0.8890	6.62E-01	-4.39E-04	7.80E-04	-0.6350	5.82E-01	-1.94E-03	3.32E-03
-1.0160	6.72E-01	-1.71E-04	3.92E-04	-0.7620	6.13E-01	-1.60E-03	2.77E-03
-1.5240	6.84E-01	1.51E-05	9.62E-05	-1.0160	6.53E-01	-7.53E-04	1.47E-03
-2.0320	6.85E-01	2.04E-05	8.96E-05	-1.2700	6.78E-01	-2.76E-04	6.34E-04
-2.5400	6.86E-01	2.15E-05	9.56E-05	-1.5240	6.86E-01	-7.48E-05	3.30E-04
-3.1750	6.87E-01	2.19E-05	9.15E-05	-1.7780	6.89E-01	2.50E-05	1.83E-04
-3.8100	6.88E-01	2.11E-05	8.71E-05	-2.0320	6.90E-01	3.36E-05	1.36E-04
-4.4450	6.90E-01	2.04E-05	8.94E-05	-2.2860	6.89E-01	2.61E-05	1.37E-04
-5.0800	6.93E-01	2.01E-05	8.31E-05	-2.5400	6.90E-01	2.08E-05	1.33E-04
				-3.0480	6.90E-01	1.99E-05	1.28E-04
				-3.5560	6.91E-01	2.29E-05	1.34E-04
				-4.0640	6.92E-01	2.46E-05	1.35E-04
				-4.5720	6.94E-01	1.89E-05	1.27E-04
				-5.0800	6.97E-01	1.28E-05	1.50E-04

TABLE 6.- BOUNDARY-LAYER PROFILES (LOWER SURFACE): MEAN AND TURBULENCE DATA
[$M_n = 0.7$; $Re_L = 40 \times 10^6$]

Y, cm	U/U_o	$-\langle uv\rangle/U_o^2$	$\langle u^2 + v^2\rangle/2U_o^2$
X = -2.86 cm			
-0.1524	5.46E-01	-5.03E-04	1.41E-03
-0.2032	5.55E-01	-5.62E-04	1.39E-03
-0.2540	5.69E-01	-4.37E-04	1.16E-03
-0.3048	5.77E-01	-4.04E-04	1.05E-03
-0.4064	5.99E-01	-3.66E-04	8.89E-04
-0.5080	6.18E-01	-2.68E-04	7.91E-04
-0.6350	6.41E-01	-1.84E-04	6.23E-04
-0.7620	6.58E-01	-1.08E-04	4.63E-04
-0.8890	6.71E-01	-6.96E-05	3.17E-04
-1.0160	6.79E-01	-1.84E-05	2.15E-04
-1.2700	6.85E-01	1.84E-05	1.64E-04
-1.5240	6.86E-01	2.38E-05	1.53E-04
-2.0320	6.84E-01	2.61E-05	1.60E-04
-2.5400	6.85E-01	3.23E-05	1.62E-04
-3.1750	6.85E-01	2.86E-05	1.64E-04
-3.8100	6.86E-01	3.13E-05	1.58E-04
-4.4450	6.87E-01	2.89E-05	1.47E-04
-5.0800	6.92E-01	9.16E-06	1.52E-04
X = -0.25 cm			
-0.2032	5.64E-01	-3.23E-04	1.29E-03
-0.2540	5.69E-01	-3.57E-04	1.13E-03
-0.3048	5.84E-01	-3.75E-04	1.13E-03
-0.4064	6.03E-01	-3.68E-04	1.04E-03
-0.5080	6.21E-01	-2.40E-04	8.31E-04
-0.6350	6.43E-01	-1.86E-04	6.21E-04
-0.7620	6.60E-01	-1.82E-04	4.77E-04
-0.8890	6.70E-01	-1.37E-04	3.47E-04
-1.0160	6.77E-01	-8.15E-05	2.49E-04
-1.5240	6.85E-01	6.43E-06	1.83E-04
-2.0320	6.83E-01	4.51E-06	1.89E-04
-2.5400	6.84E-01	1.39E-05	1.81E-04
-3.8100	6.83E-01	6.26E-06	1.69E-04
-5.0800	6.83E-01	-6.15E-06	1.80E-04

TABLE 7.- BOUNDARY-LAYER AND WAKE INTEGRAL THICKNESS PARAMETERS

[M_n = 0.7; Re_L = 40 × 10^6]

X, cm	Upper Surface		Lower Surface	
	δ^*, cm	θ, cm	δ^*, cm	θ, cm
-10.16	0.16	0.10		
-7.94	0.23	0.14		
-5.71	0.31	0.17		
-5.08	0.33	0.17		
-2.86	0.56	0.24	0.14	0.09
-2.38	0.63	0.24		
-1.27	0.82	0.26		
-0.25	1.03	0.28	0.13	0.09
0.40	0.96	0.29	0.22	0.11
0.64	0.76	0.27	0.31	0.14
1.91	0.55	0.25	0.38	0.18
5.08	0.44	0.26	0.31	0.18
7.62	0.40	0.25	0.26	0.16
12.07	0.32	0.22	0.26	0.17

Note: In the wake ($X > 0$), the integral thickness parameters for the upper and lower sides are defined about the locus of U_{min}.

TABLE 8.- SKIN-FRICTION DATA ON THE FLAP

[M_n = 0.7; Re_L = 40 × 10^6]

X, cm	c_f
-10.16	.0021
-7.94	.0011
-5.71	.0007

TABLE 9.- BOUNDARY-LAYER AND WAKE PROFILES: MEAN AND TURBULENCE DATA

[$M_n = 0.7$; $Re_L = 40 \times 10^6$]

X = -5.080 cm*				X = -2.86 cm			
Y, cm	U/U_o	$\langle u^2 \rangle / U_o^2$	$\langle v^2 \rangle / U_o^2$	Y, cm	U/U_o	$\langle u^2 \rangle / U_o^2$	$\langle v^2 \rangle / U_o^2$
5.0800	8.81E-01	2.63E-04		5.0800	8.57E-01	6.89E-04	3.48E-04
4.5720	8.82E-01	3.11E-04		4.5720	8.52E-01	5.96E-04	2.83E-04
4.0640	8.85E-01	3.69E-04		4.0640	8.52E-01	6.47E-04	2.85E-04
3.5560	8.84E-01	4.51E-04		3.5560	8.42E-01	6.96E-04	2.28E-04
3.0480	8.79E-01	6.63E-04		3.0480	8.29E-01	8.73E-04	2.44E-04
2.5400	8.77E-01	6.28E-04		2.5400	8.18E-01	9.87E-04	2.46E-04
2.2860	8.67E-01	8.52E-04		2.2860	8.03E-01	8.94E-04	1.86E-04
2.0320	8.61E-01	8.54E-04		2.0320	7.86E-01	9.04E-04	1.88E-04
1.7780	8.48E-01	9.41E-04		1.7780	7.69E-01	1.04E-03	2.13E-04
1.5240	8.31E-01	1.07E-03		1.6510	7.53E-01	1.29E-03	2.38E-04
1.3970	8.21E-01	1.30E-03		1.5240	7.44E-01	1.32E-03	2.71E-04
1.2700	8.16E-01	1.27E-03		1.2700	7.03E-01	1.83E-03	3.47E-04
1.1430	7.99E-01	1.55E-03		1.1430	7.00E-01	1.38E-03	4.15E-04
1.0160	7.88E-01	1.69E-03		1.0160	6.60E-01	2.50E-03	4.87E-04
0.8890	7.62E-01	2.02E-03		0.8890	6.31E-01	3.17E-03	6.12E-04
0.7620	7.45E-01	2.31E-03		0.7620	5.81E-01	4.61E-03	7.43E-04
0.6350	7.15E-01	2.56E-03		0.6350	5.01E-01	8.02E-03	1.21E-03
0.5080	6.78E-01	3.39E-03		0.5588	4.87E-01	8.09E-03	1.15E-03
0.4318	6.57E-01	3.70E-03		0.5080	4.05E-01	1.12E-02	1.45E-03
0.3810	6.26E-01	4.36E-03		0.4572	3.72E-01	1.17E-02	1.64E-03
0.3048	5.69E-01	5.83E-03		0.4064	3.23E-01	1.25E-02	1.88E-03
0.2540	5.24E-01	6.68E-03		0.3302	2.60E-01	1.18E-02	2.25E-03
0.2032	4.72E-01	7.66E-03		0.2540	1.95E-01	1.11E-02	2.43E-03
0.1778	4.44E-01	8.06E-03		0.2032	1.78E-01	1.02E-02	2.17E-03
0.1524	4.07E-01	8.44E-03		0.1524	1.25E-01	1.06E-02	2.21E-03
0.1270	3.82E-01	8.26E-03		0.1016	6.15E-02	9.13E-03	1.96E-03
0.1016	3.47E-01	7.97E-03					
0.0762	3.09E-01	7.80E-03					

*Single beam measurements only.

TABLE 9.- CONTINUED

X = -1.91 cm				X = -1.27 cm			
Y, cm	U/U_o	$\langle u^2\rangle/U_o^2$	$\langle v^2\rangle/U_o^2$	Y, cm	U/U_o	$\langle u^2\rangle/U_o^2$	$\langle v^2\rangle/U_o^2$
5.0800	8.36E-01	8.90E-04	3.90E-04	5.0800	8.32E-01	8.50E-04	4.82E-04
4.5720	8.37E-01	8.66E-04	3.72E-04	4.4450	8.25E-01	9.59E-04	3.18E-04
4.0640	8.33E-01	8.48E-04	2.65E-04	3.8100	8.13E-01	9.69E-04	2.45E-04
3.5560	8.22E-01	9.06E-04	2.10E-04	3.5560	8.09E-01	8.83E-04	1.90E-04
3.0480	8.10E-01	8.37E-04	1.86E-04	3.3020	8.05E-01	8.30E-04	1.64E-04
2.5400	7.86E-01	8.14E-04	1.68E-04	3.0480	8.02E-01	7.68E-04	1.78E-04
2.2860	7.76E-01	8.40E-04	1.65E-04	2.7940	7.90E-01	7.48E-04	1.19E-04
2.0320	7.58E-01	9.05E-04	2.03E-04	2.5400	7.75E-01	7.27E-04	2.23E-04
1.7780	7.43E-01	1.09E-03	2.33E-04	2.2860	7.69E-01	7.23E-04	1.56E-04
1.5240	7.07E-01	1.41E-03	3.30E-04	2.0320	7.48E-01	7.88E-04	1.78E-04
1.3970	6.94E-01	1.69E-03	3.57E-04	1.7780	7.30E-01	1.14E-03	2.54E-04
1.2700	6.67E-01	1.94E-03	4.50E-04	1.5240	6.89E-01	1.63E-03	3.59E-04
1.1430	6.48E-01	2.37E-03	5.08E-04	1.2700	6.42E-01	2.56E-03	5.66E-04
1.0160	6.11E-01	2.95E-03	7.13E-04	1.0160	5.79E-01	5.12E-03	7.69E-04
0.8890	5.71E-01	4.40E-03	8.18E-04	0.8890	5.13E-01	8.19E-03	1.10E-03
0.7620	5.07E-01	6.72E-03	1.12E-03	0.6350	3.04E-01	1.45E-02	2.17E-03
0.6350	4.30E-01	9.91E-03	1.56E-03	0.5080	2.17E-01	1.21E-02	2.62E-03
0.5080	3.11E-01	1.22E-02	2.16E-03	0.3810	1.42E-01	1.10E-02	2.86E-03
0.4064	1.91E-01	1.22E-02	2.57E-03	0.3048	9.17E-02	1.07E-02	3.02E-03
0.3556	1.50E-01	1.21E-02	2.64E-03	0.2540	6.73E-02	9.97E-03	2.93E-03
0.3048	1.27E-01	1.03E-02	2.55E-03	0.2286	4.57E-02	9.88E-03	2.66E-03
0.2540	9.71E-02	1.00E-02	2.50E-03	0.2032	3.60E-02	8.95E-03	2.59E-03
0.2032	5.05E-02	1.01E-02	3.08E-03	0.1778	2.39E-02	8.75E-03	2.68E-03
0.1778	3.22E-02	1.01E-02	2.87E-03	0.1524	6.62E-03	8.64E-03	2.39E-03
0.1524	1.98E-02	1.00E-02	2.67E-03	0.1270	-3.21E-03	7.22E-03	1.96E-03
0.1270	8.11E-03	8.74E-03	2.58E-03	0.1016	-1.03E-02	7.71E-03	4.33E-03
0.1016	-3.60E-03	8.22E-03	2.99E-03	0.0762	-2.18E-02	6.57E-03	2.93E-03

TABLE 9.- CONTINUED

X = -0.64 cm				X = -0.25 cm			
Y, cm	U/U_o	$\langle u^2\rangle/U_o^2$	$\langle v^2\rangle/U_o^2$	Y, cm	U/U_o	$\langle u^2\rangle/U_o^2$	$\langle v^2\rangle/U_o^2$
5.0800	8.23E-01	9.45E-04	2.07E-04	5.0800	8.16E-01	1.36E-03	3.23E-04
4.5720	8.20E-01	8.27E-04	1.68E-04	4.5720	8.20E-01	8.36E-04	2.18E-04
4.0640	8.10E-01	8.98E-04	1.66E-04	4.0640	8.05E-01	1.05E-03	2.07E-04
3.8100	8.02E-01	7.31E-04	1.52E-04	3.8100	7.99E-01	1.02E-03	1.90E-04
3.5560	7.95E-01	7.59E-04	1.55E-04	3.5560	7.90E-01	9.08E-04	1.92E-04
3.0480	7.77E-01	7.32E-04	1.89E-04	3.1750	7.71E-01	7.36E-04	1.75E-04
2.5400	7.57E-01	6.73E-04	1.58E-04	2.7940	7.66E-01	6.27E-04	1.58E-04
2.2860	7.44E-01	7.62E-04	2.10E-04	2.2860	7.31E-01	8.05E-04	2.73E-04
2.0320	7.28E-01	9.12E-04	2.73E-04	1.9558	7.01E-01	1.21E-03	3.04E-04
1.7780	6.94E-01	1.36E-03	3.70E-04	1.5240	6.39E-01	2.12E-03	5.72E-04
1.5240	6.53E-01	1.94E-03	4.82E-04	1.2700	5.77E-01	3.74E-03	8.42E-04
1.2700	5.94E-01	3.97E-03	8.31E-04	1.1430	4.92E-01	8.69E-03	1.47E-03
1.1430	5.16E-01	7.60E-03	1.25E-03	1.0160	4.46E-01	1.00E-02	1.59E-03
1.0160	4.49E-01	1.08E-02	1.62E-03	0.7620	3.24E-01	1.18E-02	2.31E-03
0.9144	3.80E-01	1.25E-02	2.02E-03	0.5080	1.72E-01	9.31E-03	3.11E-03
0.8128	3.03E-01	1.42E-02	2.65E-03	0.4064	9.55E-02	8.54E-03	3.09E-03
0.7620	2.99E-01	1.37E-02	2.56E-03	0.3556	7.32E-02	7.96E-03	3.18E-03
0.7112	2.43E-01	1.24E-02	2.89E-03	0.3048	5.57E-02	7.72E-03	3.18E-03
0.6096	1.70E-01	1.21E-02	3.37E-03	0.2540	2.85E-02	6.85E-03	2.44E-03
0.5080	1.31E-01	8.87E-03	3.72E-03	0.2032	9.16E-03	6.00E-03	2.10E-03
0.3810	7.83E-02	8.95E-03	3.64E-03	0.1524	-1.20E-02	5.28E-03	2.48E-03
0.3048	4.25E-02	8.14E-03	3.69E-03	0.1270	-1.78E-02	5.15E-03	2.21E-03
0.2540	1.22E-02	6.75E-03	4.19E-03	0.1016	-3.27E-02	4.30E-03	1.94E-03
0.2286	1.24E-02	6.98E-03	3.89E-03	0.0762	-3.85E-02	3.62E-03	9.96E-04
0.2032	1.29E-03	6.84E-03	3.79E-03				
0.1778	-1.15E-02	6.06E-03	3.69E-03				
0.1524	-1.87E-02	5.90E-03	3.20E-03				
0.1270	-2.44E-02	5.62E-03	3.01E-03				
0.1016	-2.73E-02	5.09E-03	2.91E-03				

TABLE 9.- CONCLUDED

X = 0.25 cm							
Y, cm	U/U_o	$\langle u^2\rangle/U_o^2$	$\langle v^2\rangle/U_o^2$				
6.3500	8.24E-01	8.91E-04	3.12E-04				
5.0800	8.16E-01	1.02E-03	2.15E-04				
4.4450	8.03E-01	8.91E-04	2.02E-04				
3.8100	7.88E-01	7.67E-04	1.85E-04				
3.0480	7.58E-01	6.75E-04	1.89E-04				
2.5400	7.36E-01	8.95E-04	2.61E-04				
2.2860	6.96E-01	1.38E-03	3.98E-04				
2.0320	6.87E-01	1.39E-03	3.96E-04				
1.7780	6.36E-01	2.49E-03	6.56E-04				
1.5240	5.77E-01	4.58E-03	1.05E-03				
1.3970	5.24E-01	8.04E-03	1.14E-03				
1.2700	4.65E-01	1.11E-02	2.06E-03				
1.1430	3.89E-01	1.28E-02	2.15E-03				
1.0160	3.07E-01	1.47E-02	3.03E-03				
0.8890	2.30E-01	1.36E-02	3.15E-03				
0.7620	1.66E-01	1.21E-02	3.74E-03				
0.6350	1.11E-01	1.17E-02	3.74E-03				
0.5080	5.01E-02	9.87E-03	3.09E-03				
0.4572	2.42E-02	9.47E-03	2.78E-03				
0.3810	-1.28E-04	7.92E-03	2.80E-03				
0.3048	-2.85E-02	6.06E-03	1.85E-03				
0.2540	-3.20E-02	5.98E-03	1.58E-03				
0.2032	-4.58E-02	3.91E-03	1.49E-03				
0.1524	-3.88E-02	2.91E-03	1.65E-03				
0.1270	-2.27E-02	3.46E-03	2.00E-03				
0.1016	6.63E-02	8.89E-03	2.01E-03				
0.0508	4.32E-01	9.77E-03	4.34E-04				
0.0000	5.21E-01	2.78E-03	3.73E-04				
0.0000	5.35E-01	2.67E-03	3.58E-04				
-0.5080	6.28E-01	1.26E-03	4.27E-03				
-0.5080	6.29E-01	1.12E-03	8.51E-03				
-0.6350	6.48E-01	8.28E-04	1.15E-02				
-0.7620	6.80E-01	5.03E-04	2.68E-03				
-1.0160	6.95E-01	2.63E-04	1.65E-04				
-1.2700	7.05E-01	7.95E-05	2.92E-04				
-1.7780	7.04E-01	9.05E-05	1.65E-04				
-2.5400	7.04E-01	8.47E-05	3.09E-04				
-5.0800	7.03E-01	6.17E-05	2.49E-04				

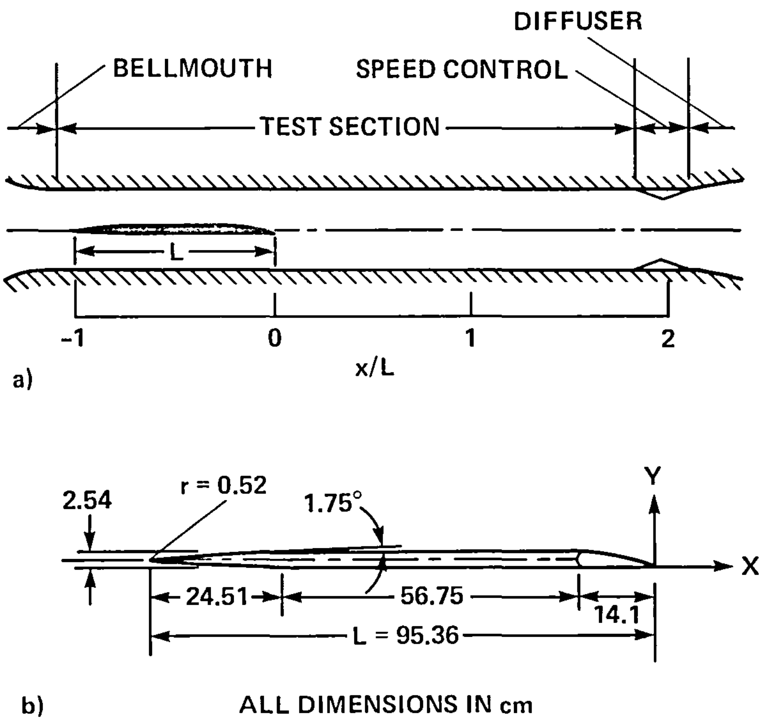

Figure 1.- Schematic of test section and test model.

(a) Test section.

(b) Test model.

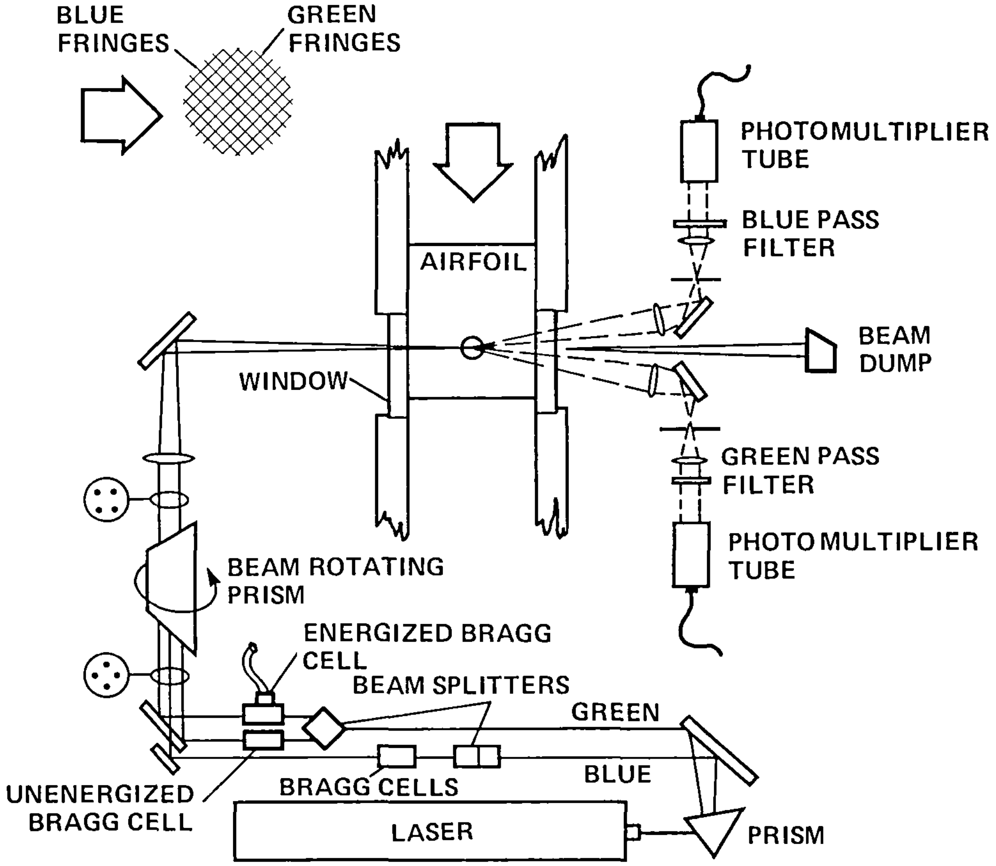

Figure 2.- Schematic of LDV optical arrangement.

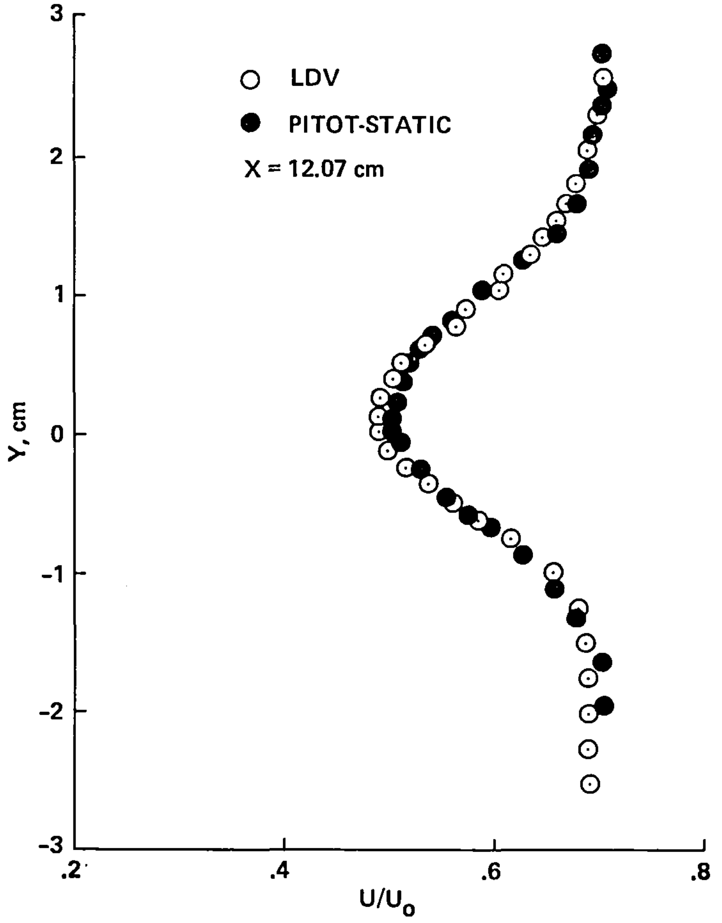

Figure 3.- Comparison of mean-velocity data from LDV and pitot-static probes: $M_n = 0.7$, $Re_L = 40 \times 10^6$.

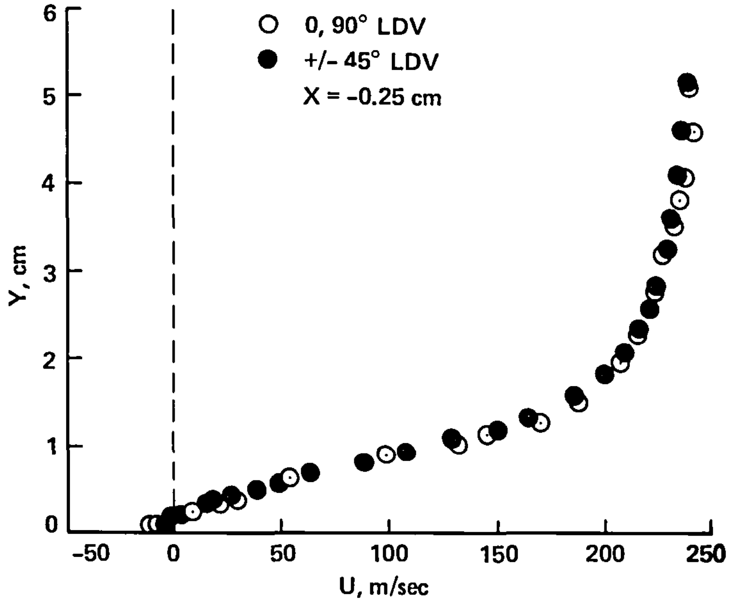

Figure 4.- Comparison of mean-velocity data obtained from two different laser beam orientations: $M_n = 0.7$, $Re_L = 40 \times 10^6$.

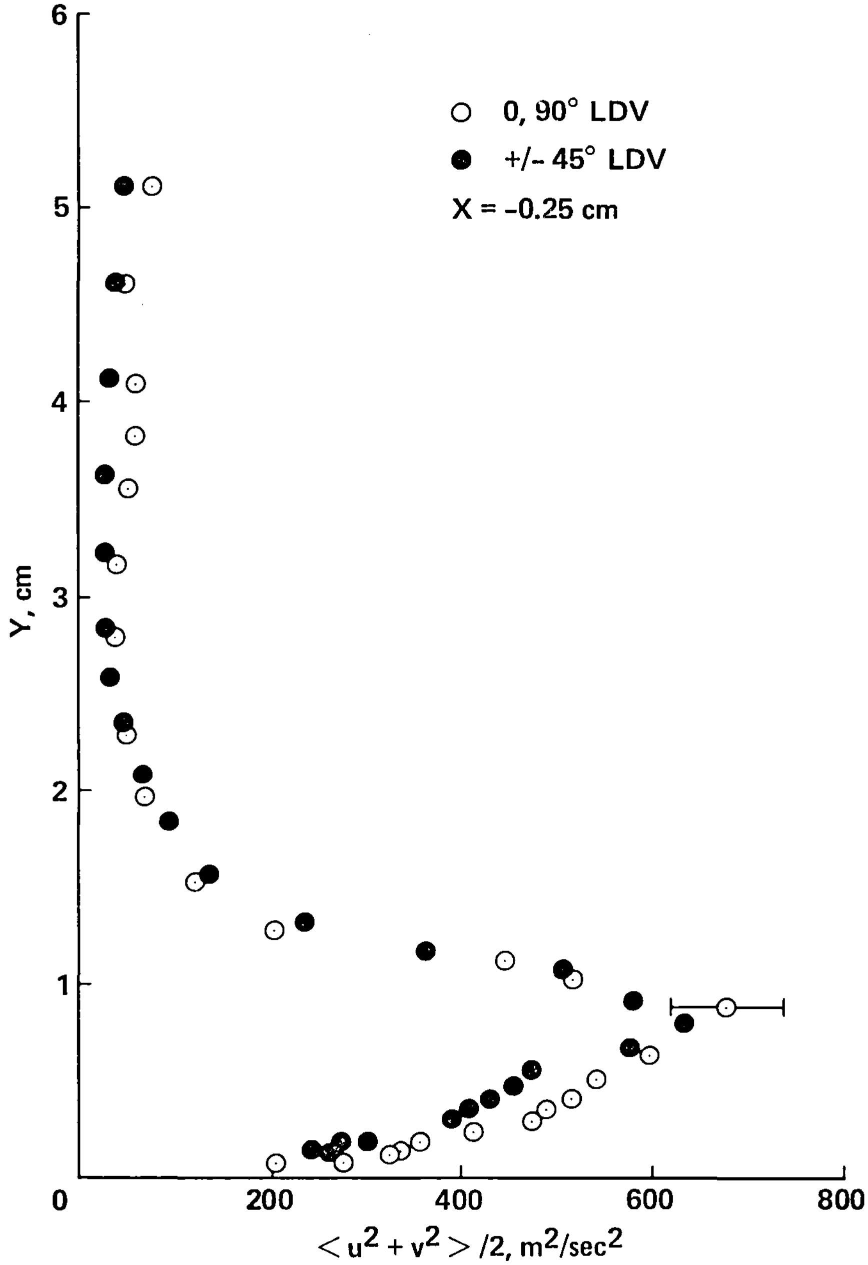

Figure 5.- Comparison of turbulent kinetic energy data obtained from two different laser beam orientations: $M_n = 0.7$, $Re_L = 40 \times 10^6$.

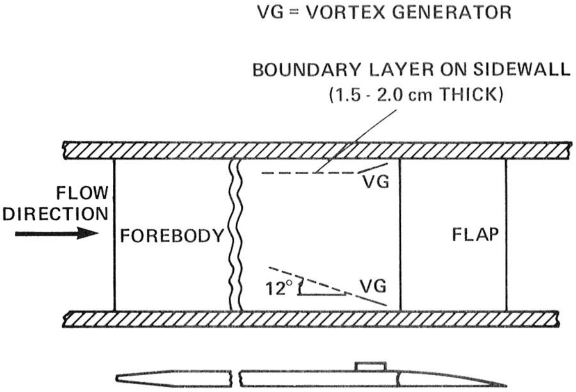

Figure 6.- Vortex generators on the model in optimum position (not to scale).

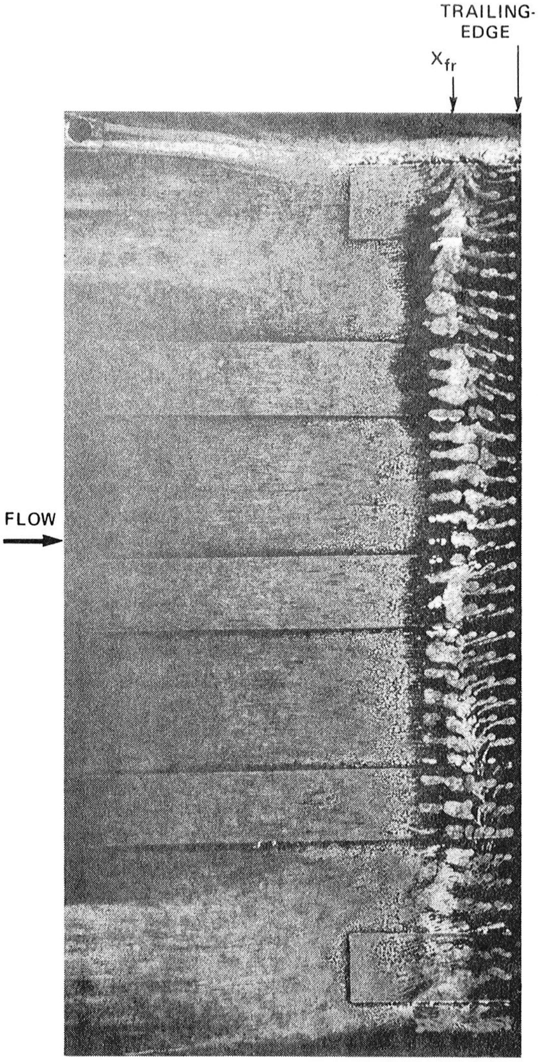

Figure 7.- Surface oil-flow pattern on the flap: $M_n = 0.7$, $Re_L = 40 \times 10^6$.

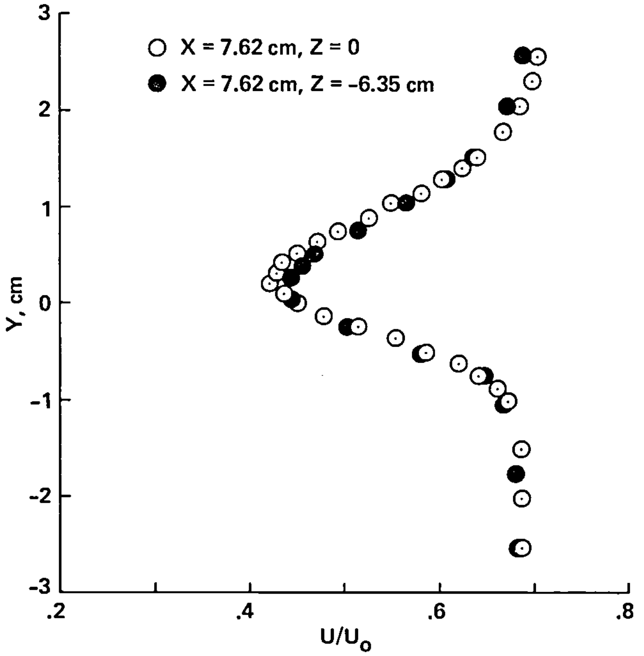

Figure 8.- Comparison of mean-velocity data on centerline and at a spanwise station: $M_n = 0.7$, $Re_L = 40 \times 10^6$.

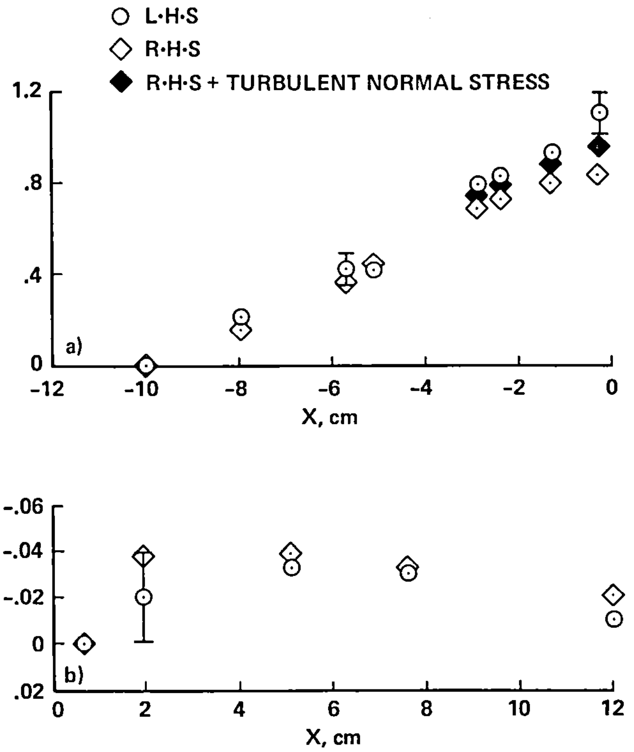

Figure 9.- Two-dimensional momentum integral balance estimates: $M_n = 0.7$, $Re_L = 40 \times 10^6$.

(a) Flap upper surface.

(b) Wake.

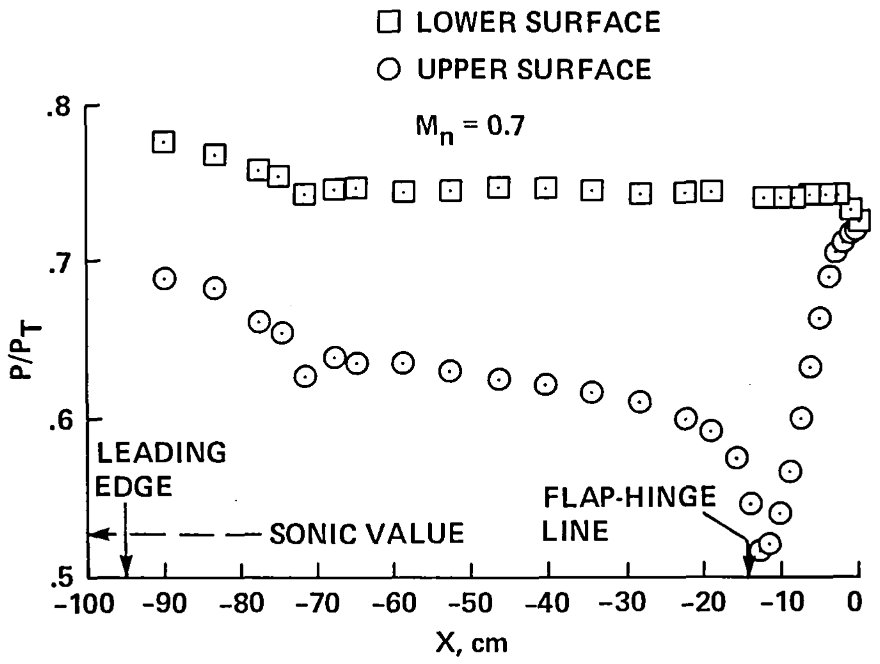

Figure 10.- Static pressure distributions on the model: $M_n = 0.7$, $Re_L = 40 \times 10^6$.

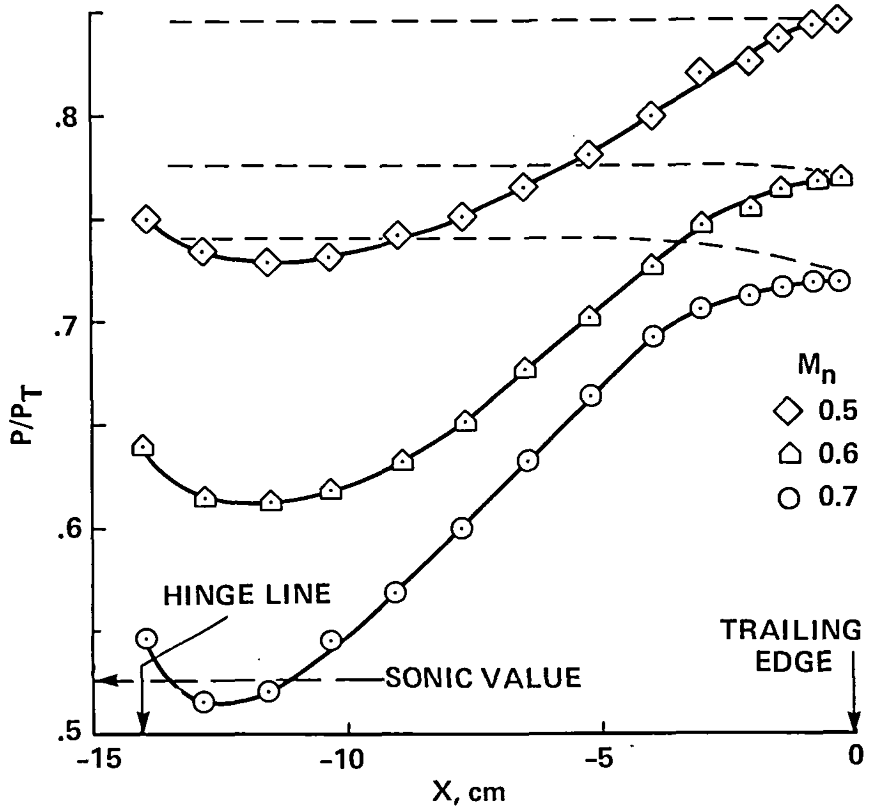

Figure 11.- Mach number effects on static pressure distributions on the flap: $P_T = 275 \times 10^3$ N/m^2.

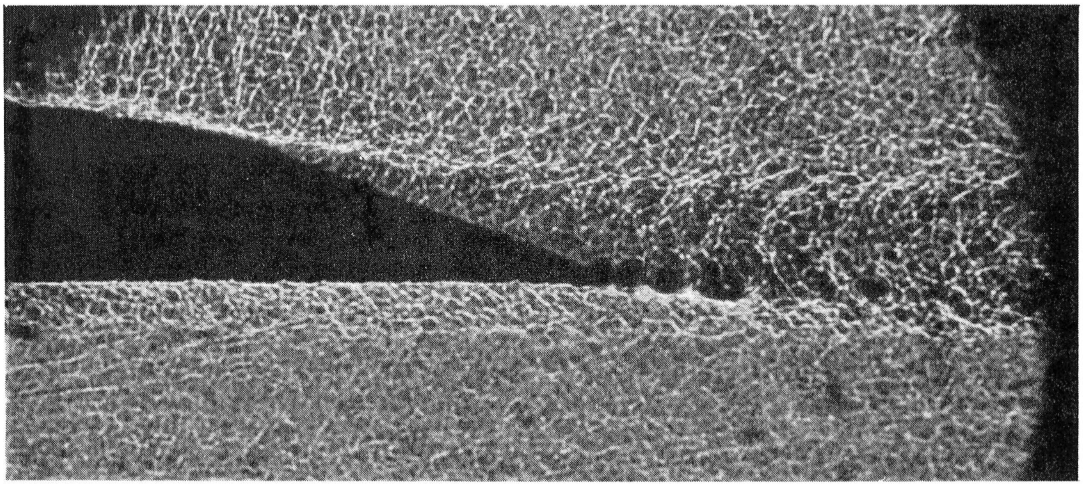

Figure 12.- Spark shadowgraph of trailing-edge flow field: $M_n = 0.7$, $Re_L = 40 \times 10^6$.

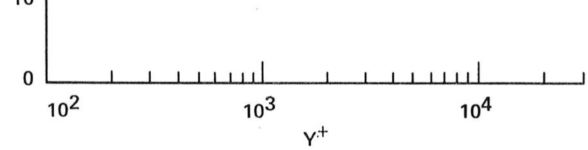

Figure 13.- Flat-plate boundary-layer velocity profile in law-of-the-wall coordinates: $M_n = 0.7$, $Re_L = 40 \times 10^6$.

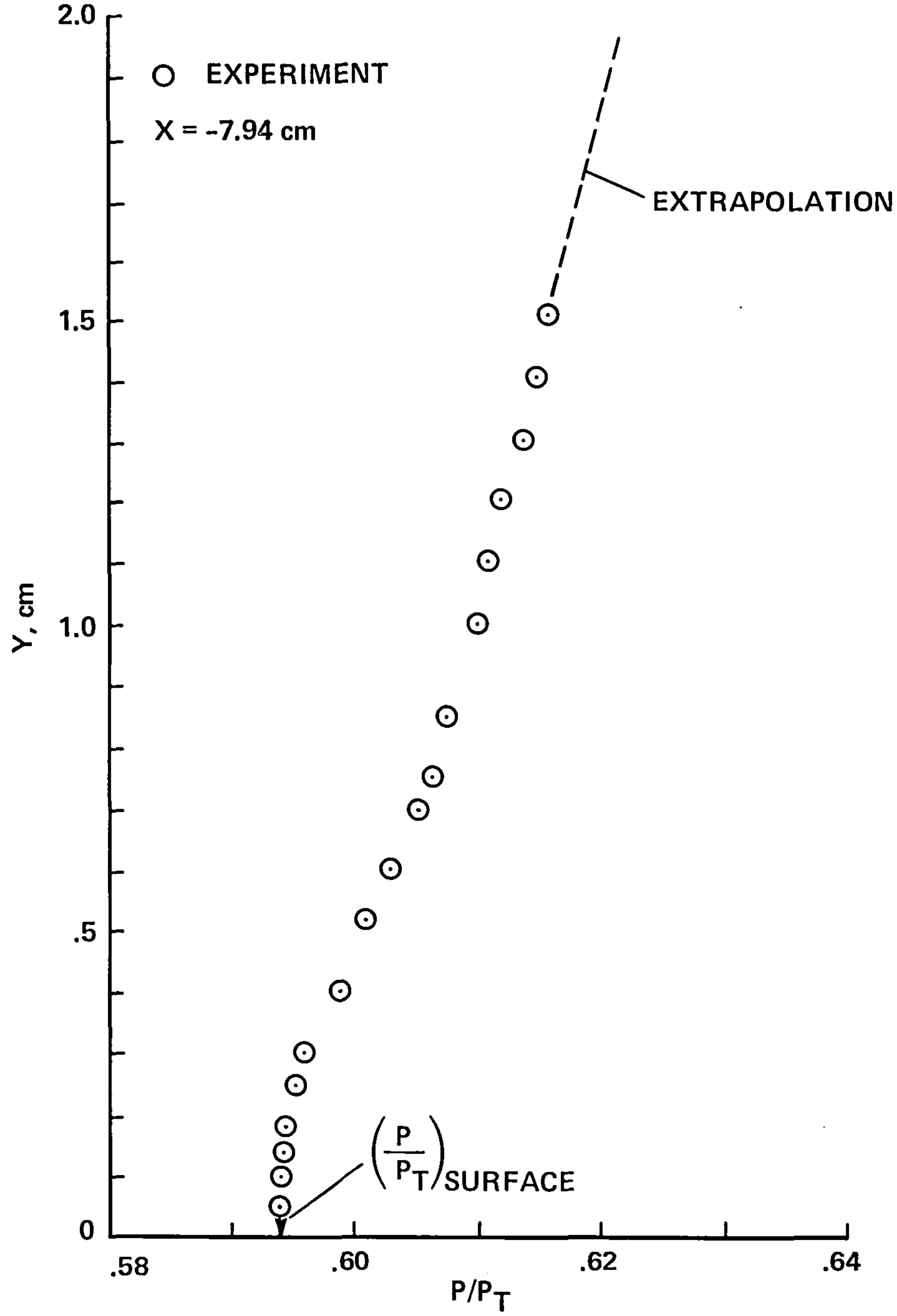

Figure 14.- Static-pressure variation across the boundary layer: $M_n = 0.7$, $Re_L = 40 \times 10^6$.

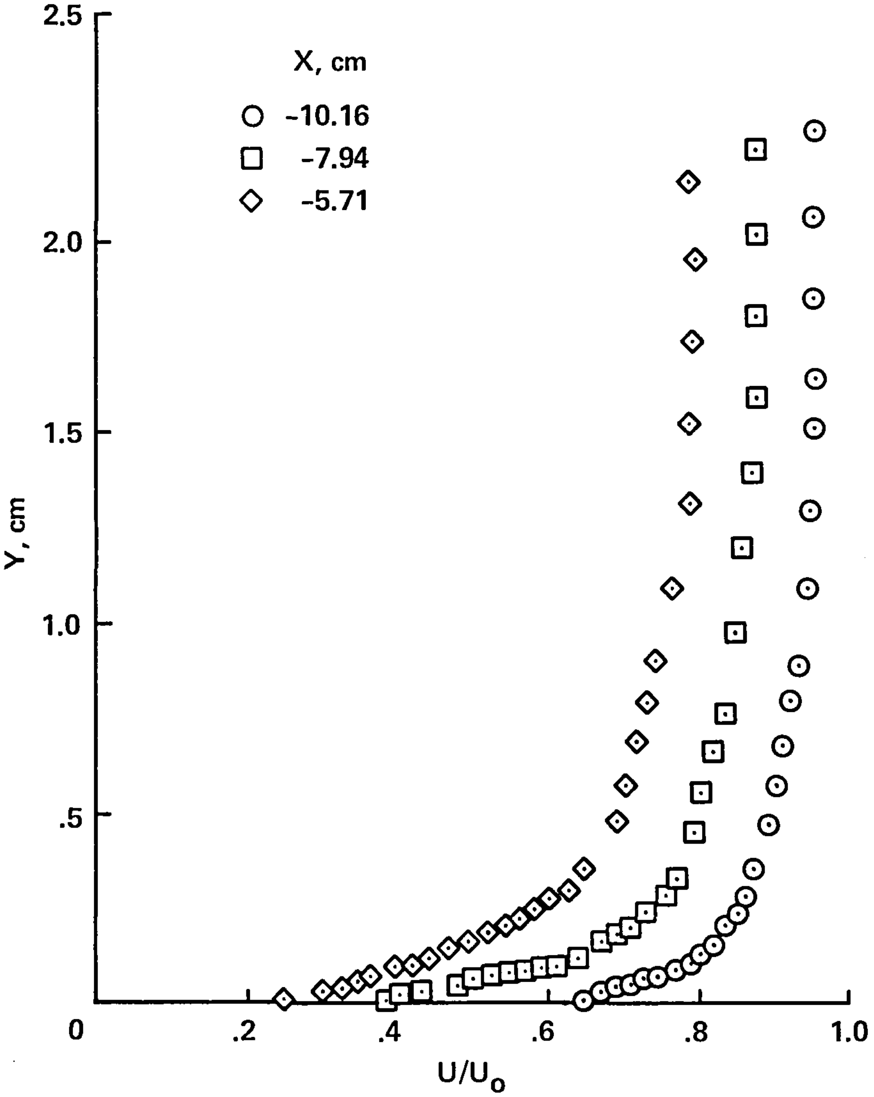

Figure 15.- Mean velocity profiles ahead of separation $M_n = 0.7$, $Re_L = 40 \times 10^6$.

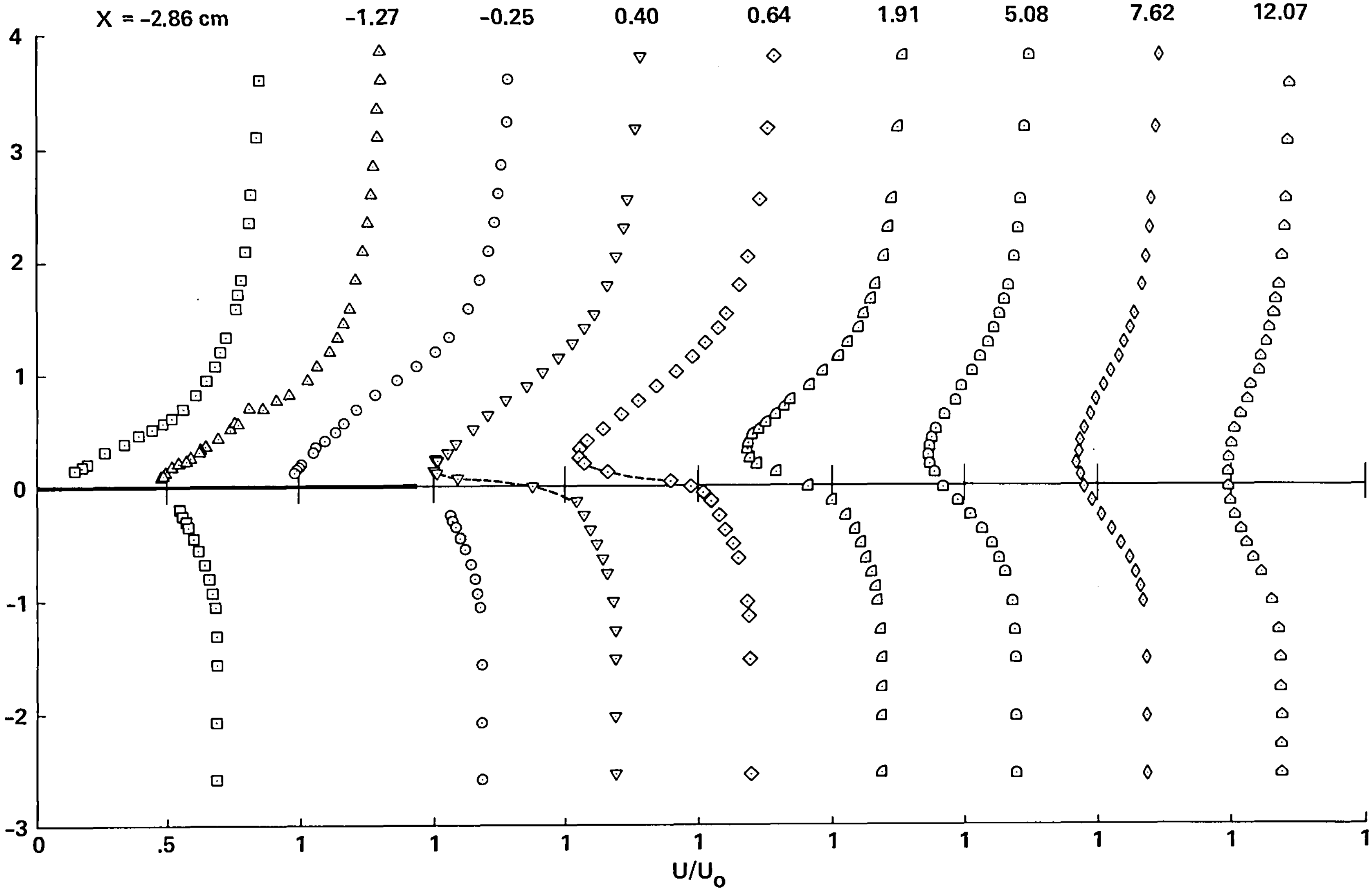

Figure 16.- Mean velocity profiles in the separated region and in the near-wake: $M_n = 0.7$, $Re_L = 40 \times 10^6$.

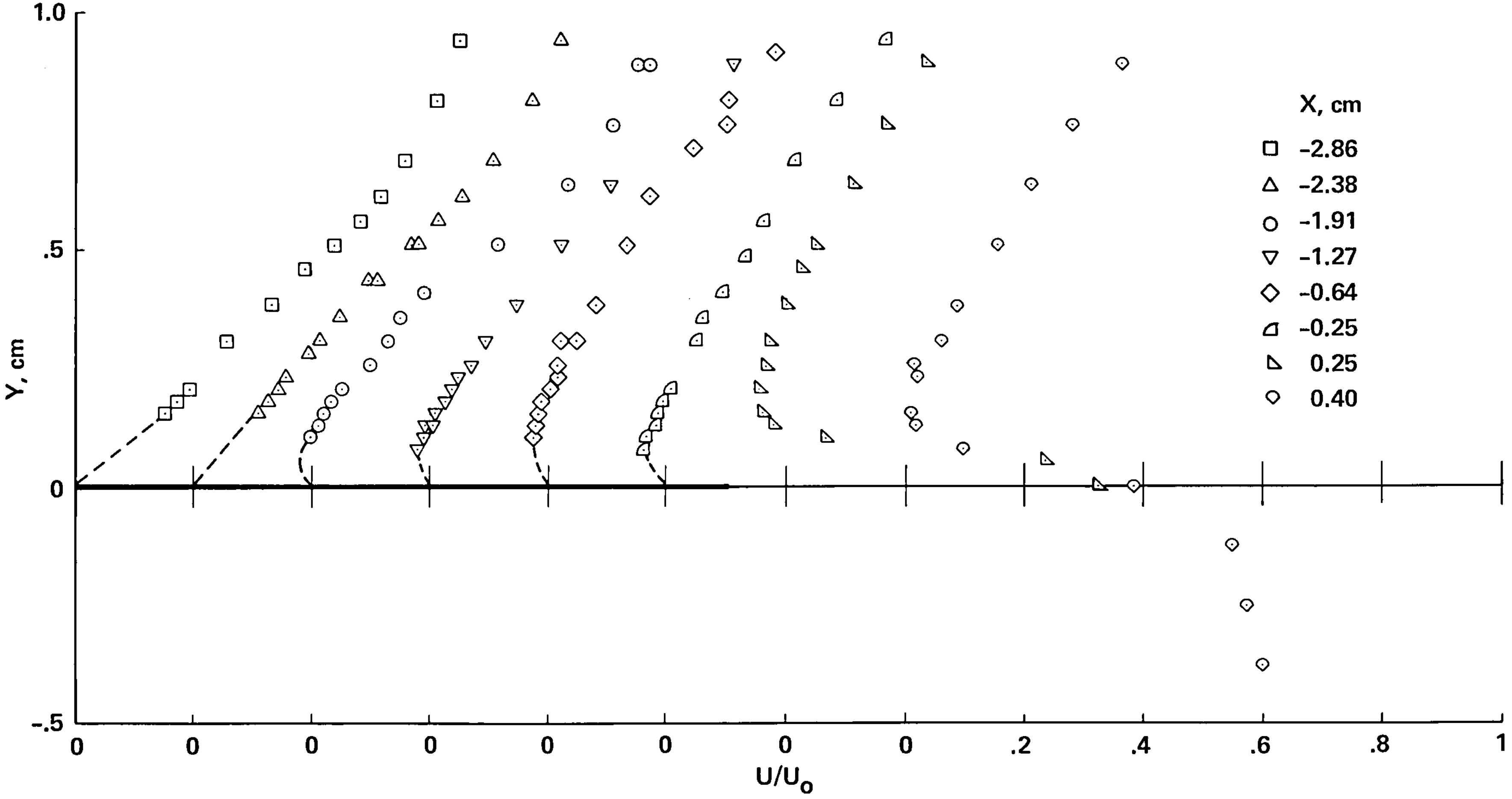

Figure 17.- Mean-velocity profiles in the separated zone: $M_n = 0.7$, $Re_L = 40 \times 10^6$.

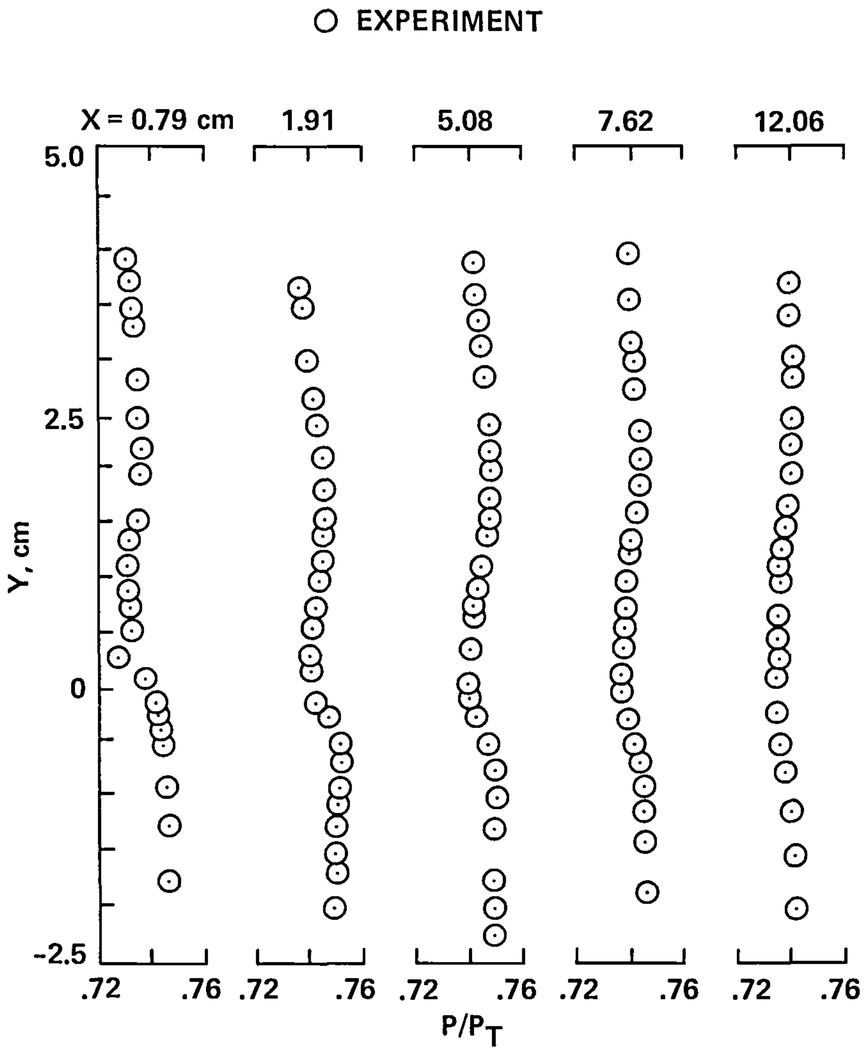

Figure 18.- Static-pressure variations across the near-wake: $M_n = 0.7$, $Re_L = 40 \times 10^6$.

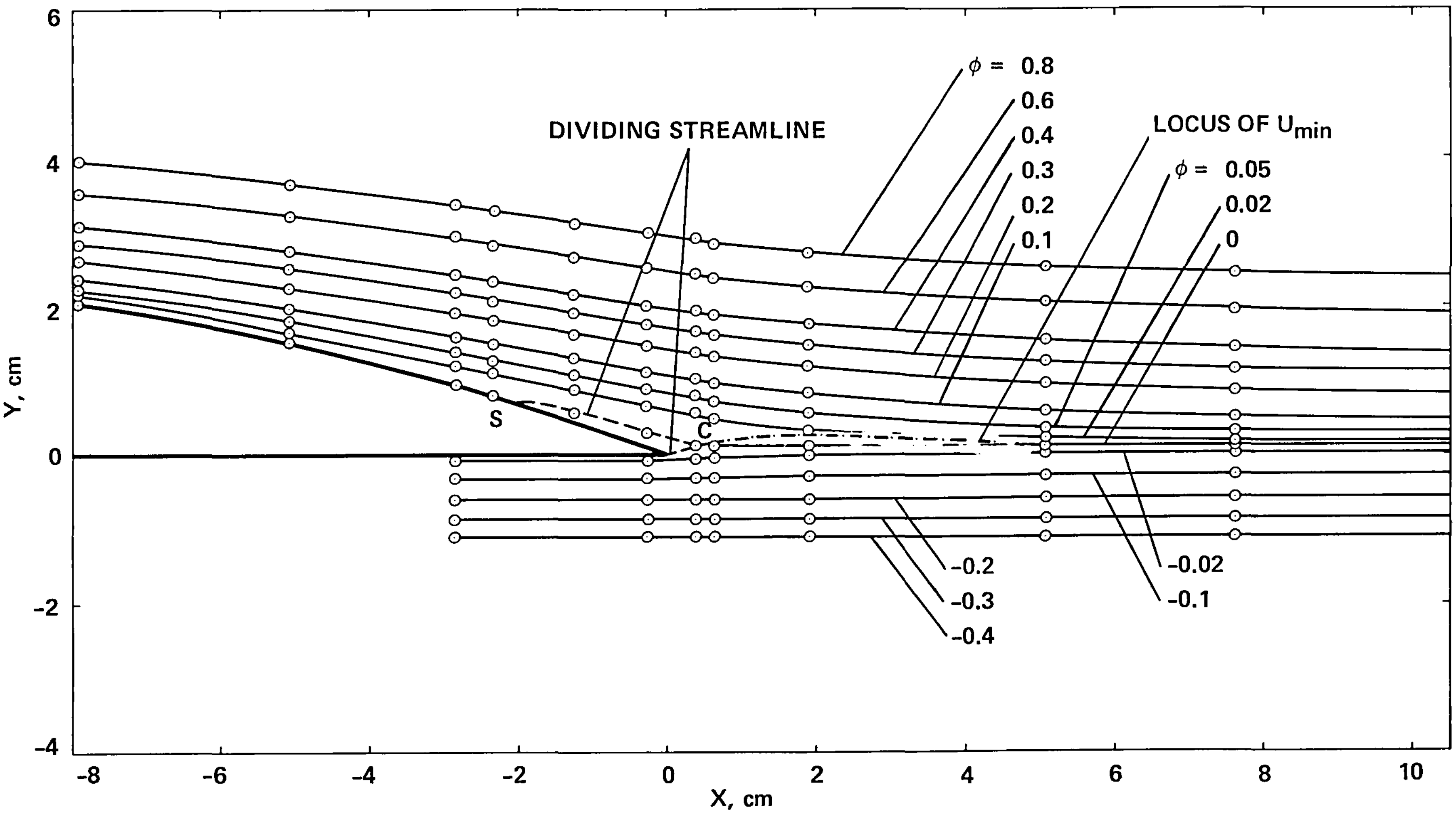

Figure 19.- Mean stream-function contours above the flap and in the near wake: $M_n = 0.7$, $Re_L = 40 \times 10^6$.

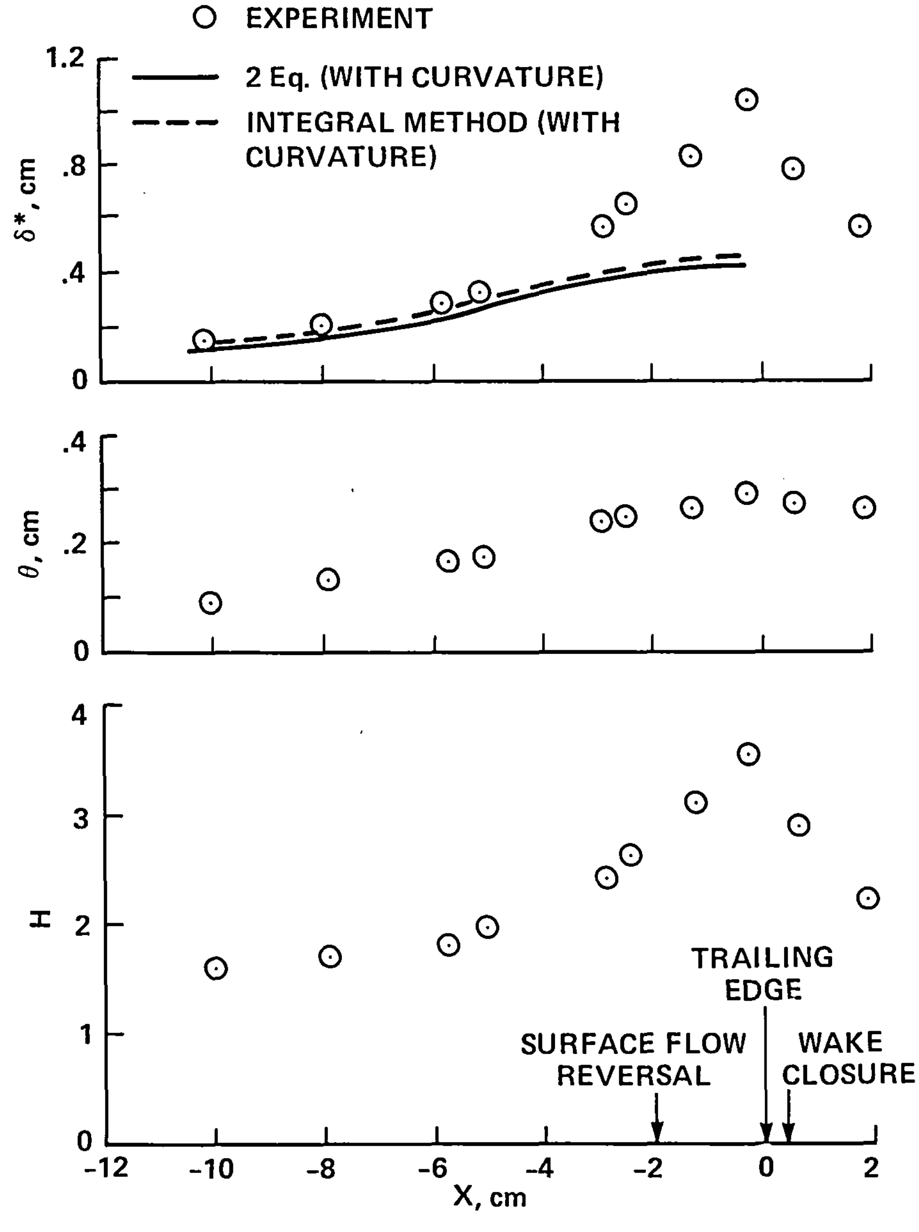

Figure 20.- Variation of boundary-layer integral thickness parameters above the flap: $M_n = 0.7$, $Re_L = 40 \times 10^6$.

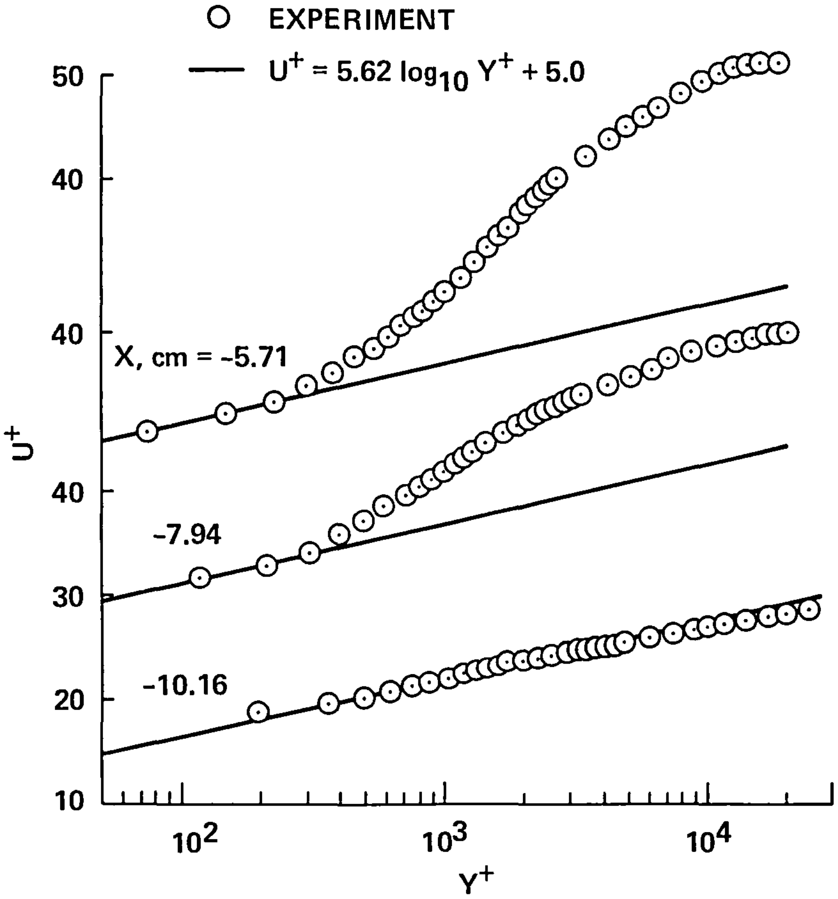

Figure 21.- Flow boundary-layer velocity profiles in law-of-the-wall coordinates: $M_n = 0.7$, $Re_L = 40 \times 10^6$.

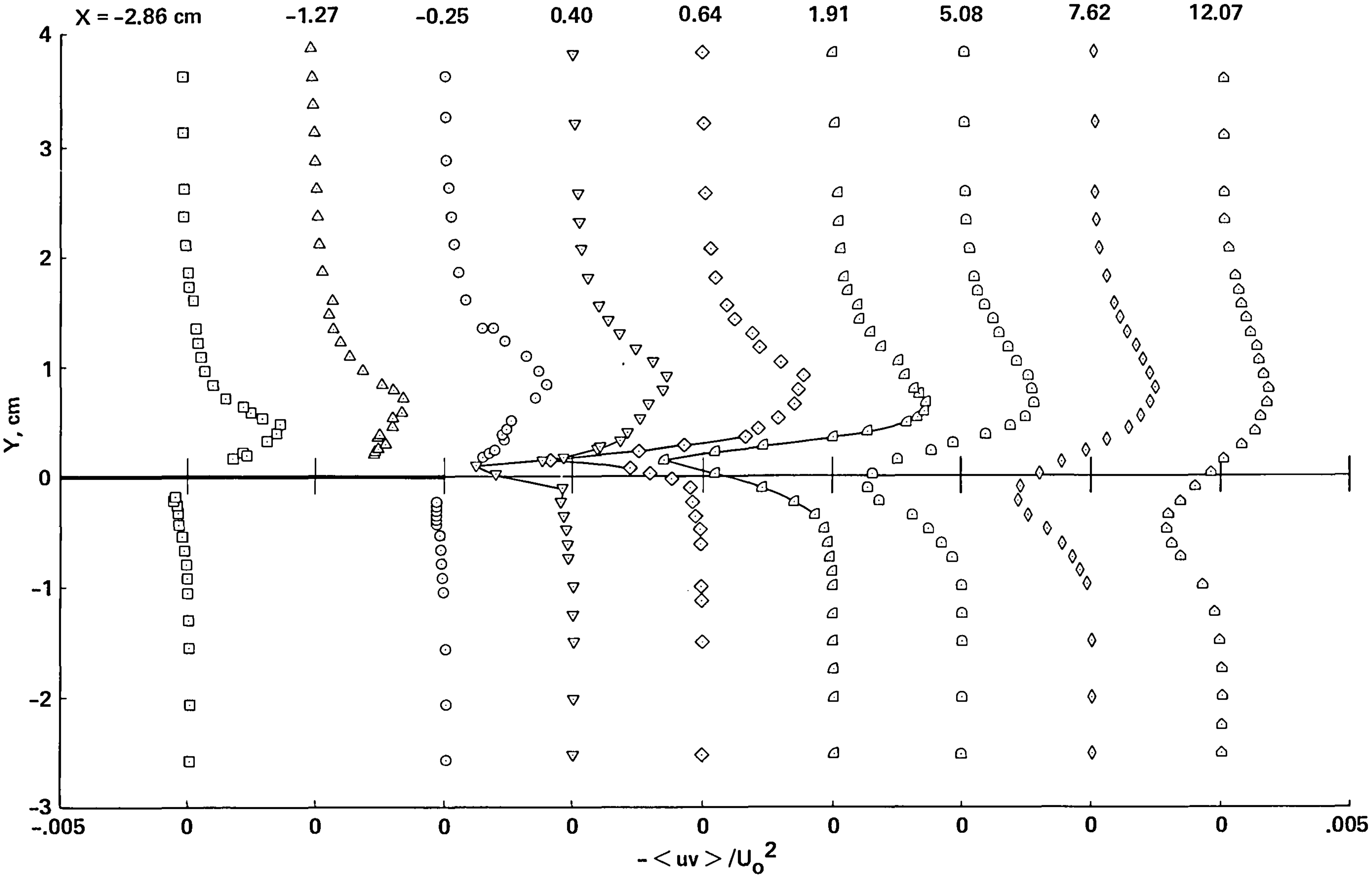

Figure 22.- Turbulent shear-stress profiles in the separated region and in the near-wake: $M_n = 0.7$, $Re_L = 40 \times 10^6$.

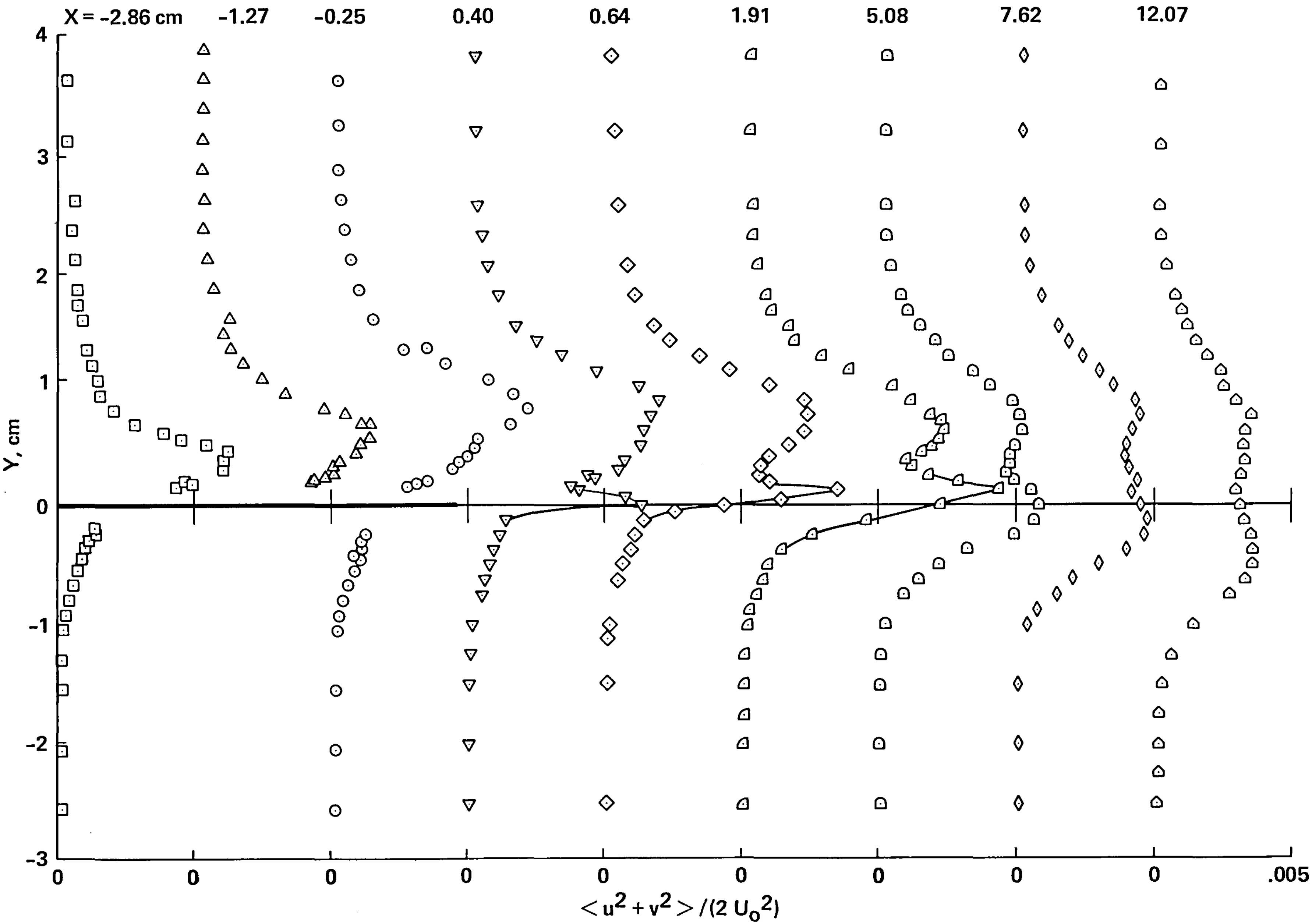

Figure 23.- Turbulent kinetic-energy profiles in the separated region and in the near-wake: $M_n = 0.7$, $Re_L = 40 \times 10^6$.

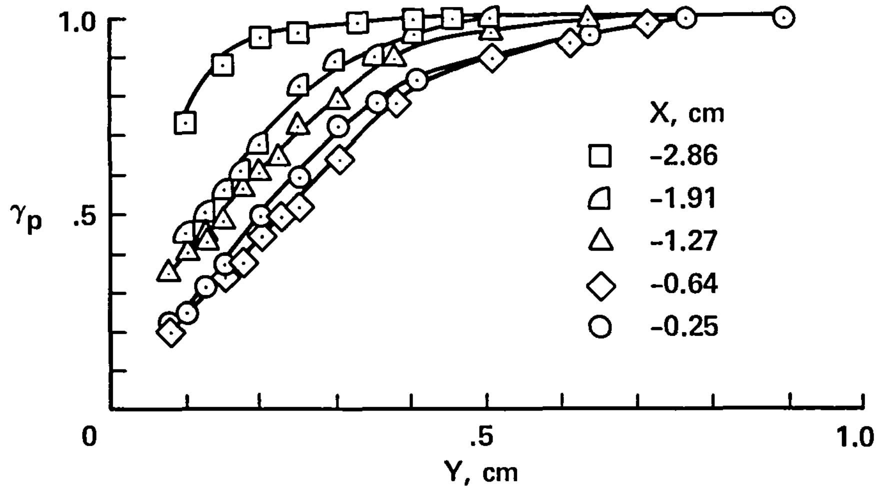

Figure 24.- γ_p distributions ahead of separation and in the separated region: $M_n = 0.7$, $Re_L = 40 \times 10^6$.

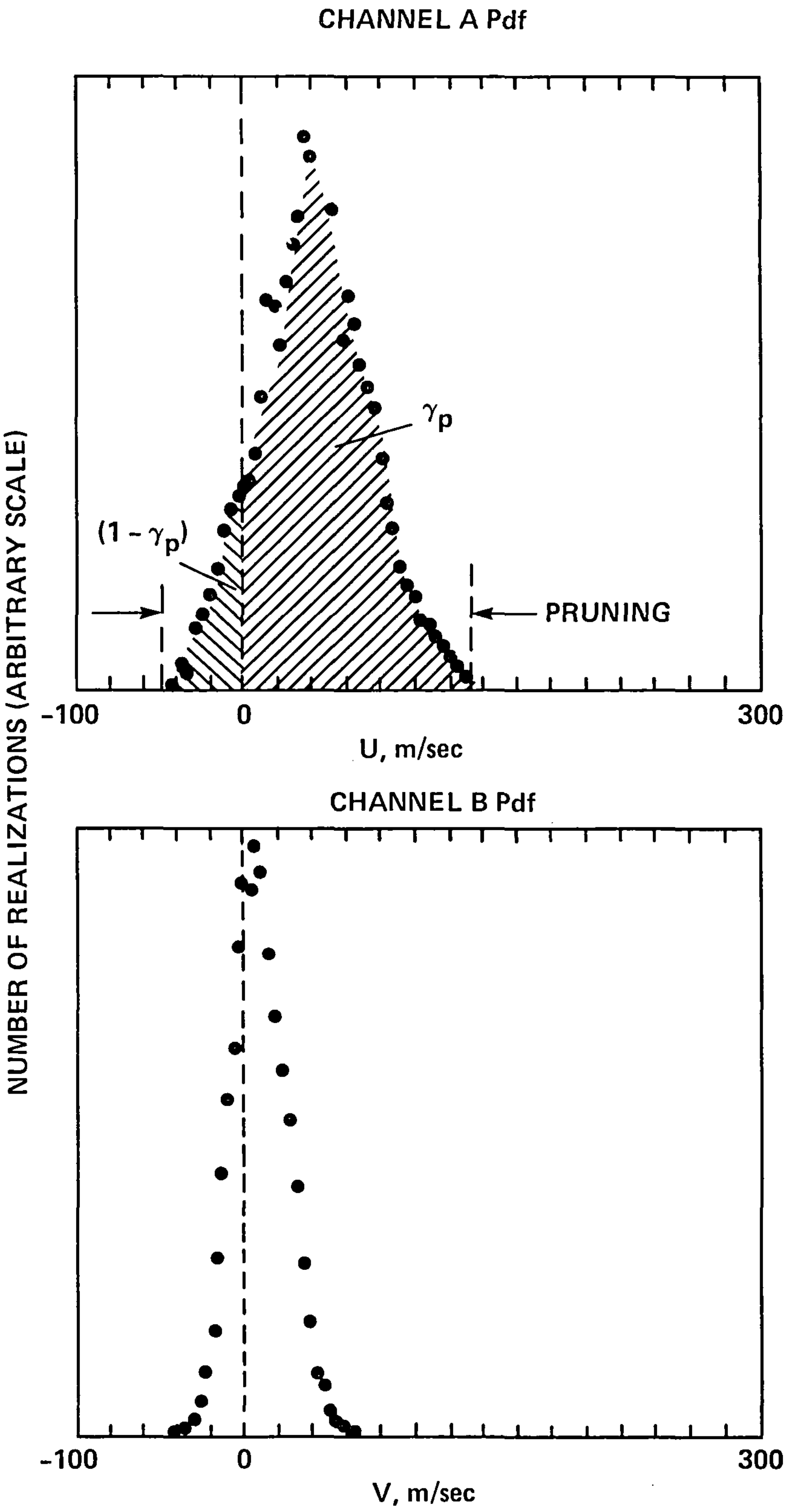

Figure 25.- Typical histograms of LDV measurements.

1. Report No. NASA TM 84290	2. Government Accession No.	3. Recipient's Catalog No.

4. Title and Subtitle AN EXPERIMENTAL DOCUMENTATION OF A SEPARATED TRAILING-EDGE FLOW AT A TRANSONIC MACH NUMBER	5. Report Date November 1982 6. Performing Organization Code
7. Author(s) P. R. Viswanath and J. L. Brown	8. Performing Organization Report No. A-9074 10. Work Unit No. T-4217
9. Performing Organization Name and Address NASA Ames Research Center Moffett Field, Calif. 94035	11. Contract or Grant No. 13. Type of Report and Period Covered Technical Memorandum
12. Sponsoring Agency Name and Address National Aeronautics and Space Administration Washington, D. C. 20546	14. Sponsoring Agency Code 505-31-11

15. Supplementary Notes

Point of contact: P. R. Viswanath, Ames Research Center, MS 229-1
Moffett Field, CA 94035 (415) 965-6211

16. Abstract

A detailed experiment on the separated flow field at a sharp trailing edge is described and documented. The separated flow is a result of sustained adverse pressure gradients. The experiment was conducted using an elongated airfoil-like model at a transonic Mach number and at a high Reynolds number of practical interest. Measurements made include surface pressures and detailed mean and turbulence flow quantities in the region just upstream of separation to downstream into the near-wake, following wake closure. The data obtained are presented mostly in tabular form. These data are of sufficient quality and detail to be useful as a test case for evaluating turbulence models and calculation methods.

17. Key Words (Suggested by Author(s)) Boundary layer Wake Transonic flow	18. Distribution Statement Unlimited Subject Category - 34

19. Security Classif. (of this report) Unclassified	20. Security Classif. (of this page) Unclassified	21. No. of Pages 50	22. Price* A03

*For sale by the National Technical Information Service, Springfield, Virginia 22161